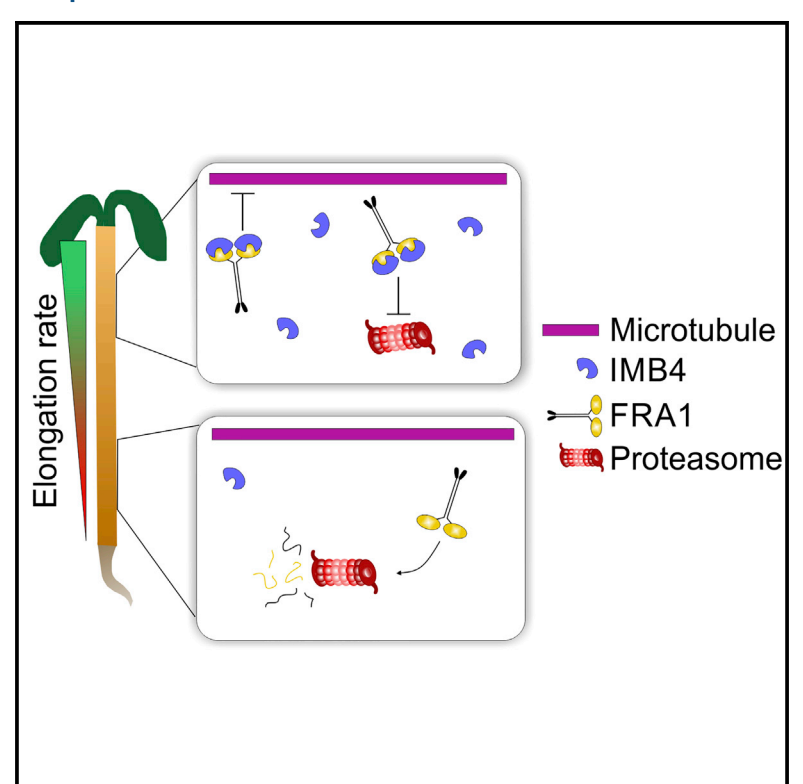
Developmental Cell

Importin- β Directly Regulates the Motor Activity and Turnover of a Kinesin-4

Graphical Abstract



Authors

Anindya Ganguly, Logan DeMott, Chuanmei Zhu, Daniel D. McClosky, Charles T. Anderson, Ram Dixit

Correspondence

ramdixit@wustl.edu

In Brief

How the activity of kinesins is regulated to meet cellular needs remains poorly understood. Ganguly et al. show that the motility and proteasome-mediated degradation of a kinesin-4 is regulated in a developmental manner by the binding of an importin- β to a conserved PY motif in the kinesin motor domain.

Highlights

- The importin-β IMB4 directly binds to a PY motif in the FRA1 kinesin motor domain
- IMB4 protects FRA1 from proteasome-mediated degradation in a developmental manner
- IMB4 also inhibits the microtubule binding ability of the FRA1 motor domain
- The IMB4 binding PY motif is conserved in multiple kinesin families





Importin-β Directly Regulates the Motor Activity and Turnover of a Kinesin-4

Anindya Ganguly, ¹ Logan DeMott, ^{1,3} Chuanmei Zhu, ^{1,4} Daniel D. McClosky, ² Charles T. Anderson, ² and Ram Dixit^{1,5,*} ¹Department of Biology and Center for Engineering Mechanobiology, Washington University in St. Louis, 1 Brookings Drive, CB 1137, St. Louis, MO 63130, USA

²Department of Biology and Center for Lignocellulose Structure and Formation, The Pennsylvania State University, University Park, PA 16802, USA

³Present address: Department of Plant Sciences, University of California, Davis, CA 95616, USA

⁴Present address: Donald Danforth Plant Science Center, St. Louis, MO 63132, USA

⁵Lead Contact

*Correspondence: ramdixit@wustl.edu https://doi.org/10.1016/j.devcel.2018.01.027

SUMMARY

Spatiotemporal regulation of kinesins is essential for microtubule-dependent intracellular transport. In plants, cell wall deposition depends on the FRA1 kinesin, whose abundance and motility are tightly controlled to match cellular growth rate. Here, we show that an importin-β, IMB4, regulates FRA1 activity in a developmental manner. IMB4 physically interacts with a PY motif in the FRA1 motor domain and inhibits its motility by preventing microtubule binding, while also protecting FRA1 against proteasome-mediated degradation, thus providing a mechanism to couple the motility and stability of FRA1. This regulatory mechanism is likely to be broadly applicable, based on the conservation of the PY motif in the motor domains of plant and animal kinesins and the direct interaction of multiple plant kinesins with IMB4. Together, our data establish IMB4 as a multi-functional regulator of FRA1 and reveal a mechanism for how plants control the magnitude of cargo transport needed for cell wall assembly.

INTRODUCTION

Kinesins are ATP-powered molecular motors that drive the directional transport of cellular cargo along microtubules (MTs). In cells, the majority of kinesins diffuse in the cytoplasm, and only a small fraction of them bind to and move processively along MTs at any given time (Cai et al., 2007a; Zhu et al., 2015). This is because transport kinesins are kept in an inactive state when not coupled to cargo, likely to conserve cellular ATP and to prevent crowding of MT tracks by cargoless kinesins. Inactivation of kinesin-1, -2, -3, and -7 families involves autoinhibition through interaction of the cargo-binding tail domain or other internal domains with the motor domain (Coy et al., 1999; Dietrich et al., 2008; Friedman and Vale, 1999; Hackney et al., 2009; Hammond et al., 2009, 2010; Imanishi et al., 2006). In the case of kinesin-1, kinesin light chains bound to the tail domain also

contribute to motor inactivation (Cai et al., 2007b; Verhey et al., 1998). Autoinhibition can be overcome either by the binding of cargo to the tail domain or kinesin light chain (Blasius et al., 2007; Sun et al., 2011), or by phosphorylation of the tail domain (Cahu et al., 2008; Espeut et al., 2008), thus enabling cargo transport.

Regulation of kinesin turnover is another mechanism to control kinesin-driven transport. This mechanism is particularly prevalent during mitosis, when degradation by the 26S proteasome system sharply reduces the activity of various kinesins at specific stages of mitosis (Funabiki and Murray, 2000; Gordon and Roof, 2001; Hildebrandt and Hoyt, 2001; Malcos and Cyr, 2011; Senese et al., 2015). Together, these regulatory mechanisms determine the efficiency and volume of cargo transport by kinesins.

Recently, an Arabidopsis thaliana kinesin-4, called Fragile Fiber 1 (FRA1), was shown to be important for cell wall production (Zhong et al., 2002; Kong et al., 2015; Zhu et al., 2015). FRA1 moves processively on cortical MTs and is thought to transport Golgi-derived vesicles containing noncellulosic cell wall components for secretion (Kong et al., 2015; Zhu et al., 2015). Consistent with a transport function, a high level of processive motility was found to be critical for the function of FRA1 (Ganguly et al., 2017). Interestingly, plants regulate the abundance and motility of FRA1 such that FRA1 activity is high in rapidly growing tissues (Zhu et al., 2015), presumably to ensure the high rates of cell wall secretion that are required for cellular expansion. However, the molecular mechanisms that dynamically regulate the magnitude of FRA1-based transport over the course of growth and development are unknown.

Here, we identify an importin- β , IMB4, as a key regulator of the motility and turnover of the FRA1 kinesin. We show that IMB4 interacts directly with the motor domain of FRA1 through a PY motif, which inhibits FRA1 motility by preventing the binding of FRA1 to MTs and also enhances the lifetime of FRA1 by preventing the degradation of FRA1 by the proteasome system. We also demonstrate that the motor domains of multiple mitotic plant kinesins bind directly to IMB4. Based on our data, we conclude that importin- β -mediated regulation of kinesin motility is likely to be a conserved mechanism for both interphase and mitotic kinesins



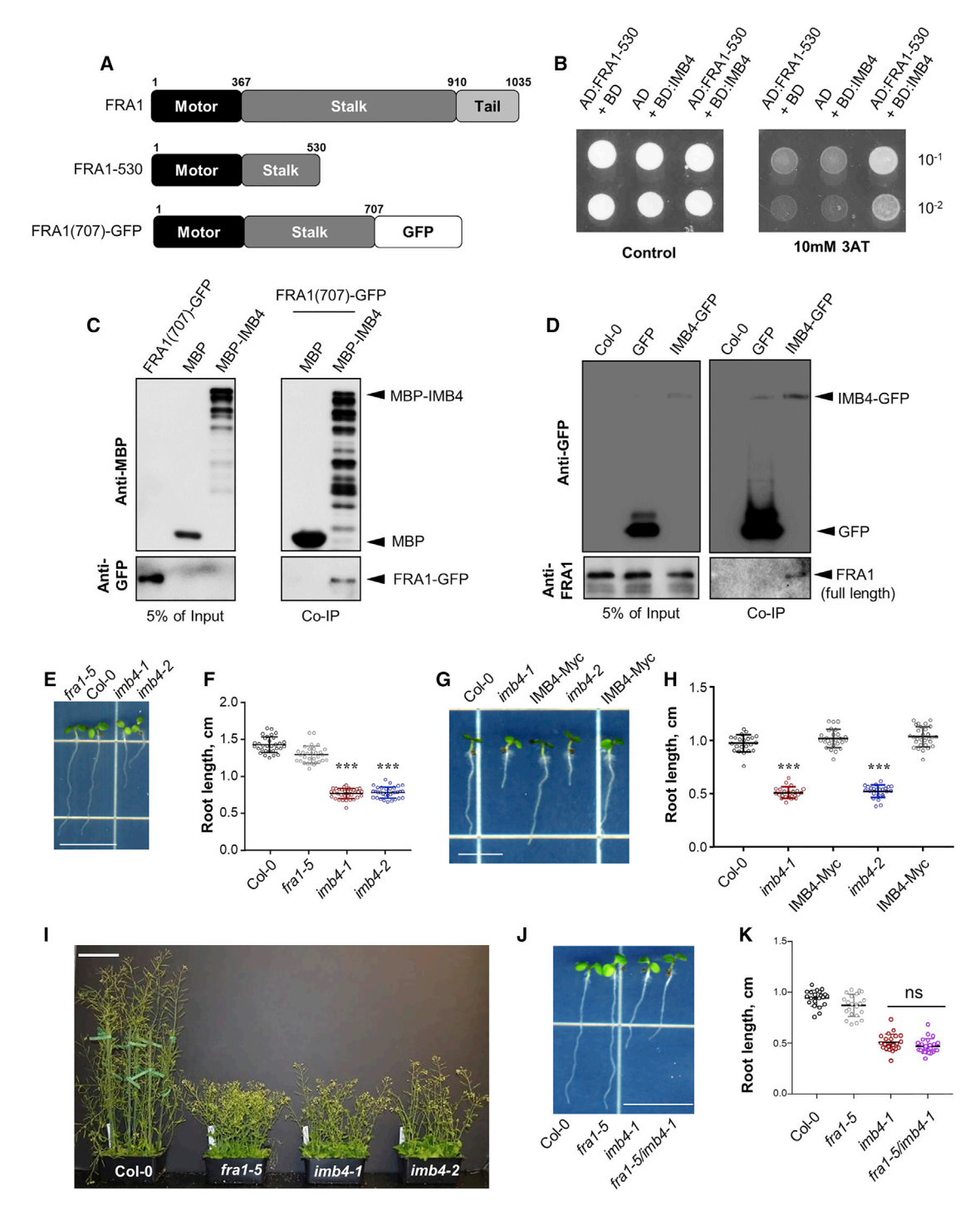


Figure 1. IMB4 Interacts Directly with FRA1

- (A) Schematic representation of the FRA1 proteins used in this study.
- (B) Yeast two-hybrid assay using the FRA1 motor domain (amino acids 1–530), fused with the activation domain (AD) as prey and IMB4 fused with the DNA binding domain (BD) as bait.
- (C) In vitro pull-down experiment with either MBP alone or MBP-tagged IMB4 incubated with equal amounts of FRA1(707)-GFP. Immunoblotting was performed with the indicated antibodies to detect the IMB4 and FRA1 proteins.
- (D) *In vivo* pull-down experiment using anti-GFP agarose beads to pull-down either GFP alone or IMB4-GFP expressed in Col-0 plants. The resulting proteins were probed with the indicated antibodies.
- (E and F) Root lengths of 4-day-old light-grown seedlings. Values are means \pm SD (n > 30 seedlings).
- (G and H) Root lengths of 3-day-old light-grown seedlings. Values are means \pm SD (n > 30 seedlings).
- (I) Morphology of plants 42 days after germination in continuous light. Scale bar, 5 cm.

RESULTS

The Importin- β Protein, IMB4, Physically Interacts with the FRA1 Kinesin

A yeast two-hybrid assay with the FRA1 kinesin (At5g47820) showed that the FRA1 N-terminal motor domain (amino acids 1–530) (Figure 1A) interacts directly with an *Arabidopsis* importin-β (At4g27640) (Figure 1B). Based on its homology with the human importin-4β, this protein was named IMB4 in *Arabidopsis* (Tamura and Hara-Nishimura, 2014). To confirm this interaction, we performed *in vitro* pull-down experiments and found that full-length, MBP-tagged IMB4 pulled down the FRA1 motor domain, whereas MBP alone did not (Figure 1C). To determine whether this interaction occurs *in vivo*, we immunoprecipitated GFP-tagged IMB4 that was overexpressed in wild-type *Arabidopsis thaliana* plants and found that IMB4-GFP, but not GFP alone, pulls down endogenous FRA1 (Figure 1D). Together, these results identify IMB4 as an interaction partner of the FRA1 kinesin.

Loss-of-Function *imb4* Mutants Show Developmental Defects

To explore the function of IMB4, we obtained two independent transfer DNA insertion mutants of IMB4, which we named *imb4-1* and *imb4-2* (Figure S1A). Both mutants had significantly reduced *IMB4* expression compared with wild-type plants, indicating that they are likely to be loss-of-function mutants (Figure S1B).

Both *imb4* mutants showed similar developmental defects in seedlings and adult plants. The roots of light-grown *imb4* seedlings and the hypocotyls of dark-grown *imb4* seedlings were ~50% shorter than those of wild-type, respectively (Figures 1E, 1F, and S1C). The *imb4* mutants had significantly shorter cells in the root elongation zone and showed abnormal cell division planes and abnormal cellular organization in the meristematic zone compared with wild-type (Figures S1D and S1E). The combination of defective elongation and cell division in the *imb4* mutants provides a potential explanation for their more severe seedling growth defects compared with the *fra1-5* mutant (Figures 1E and S1C), which affects only elongation (Zhu et al., 2015).

In the adult stage, both *imb4* mutants showed a dwarf phenotype similar to the *fra1-5* mutant (Figures 1I and S1F). Siliques and rosette leaves were similarly small in the *imb4-1*, *imb4-2*, and *fra1-5* mutants compared with wild-type (Figures S1G–S1I). However, unlike the *fra1-5* mutant, the *imb4* mutants show delayed emergence of primary inflorescence stems (Figure S1J) and only slightly lower stem growth rates than wild-type (Figure S1F). Importantly, expression of a Myc epitope-tagged, full-length IMB4 under the control of the native *IMB4* promoter fully restored the seedling and adult growth of both *imb4* mutants to wild-type levels (Figures 1G, 1H, S2A, and S2B), thus demonstrating that the growth defects in the *imb4* mutants were due to the loss of IMB4 function alone.

To determine the functional relationship between FRA1 and IMB4, we created an *imb4-1 fra1-5* double mutant. Quantitative analyses of *fra1-5*, *imb4-1*, and *imb4-1 fra1-5* mutants showed that the growth and developmental defects of the *imb4-1 fra1-5* double mutant were indistinguishable from the *imb4-1* single mutant in seedlings and adult plants (Figures 1J, 1K, and S2C–S2I), indicating that FRA1 and IMB4 are probably acting in the same pathway.

IMB4 Regulates the Degradation of FRA1 via the 26S Proteasome System

Since importins can transport transcription factors into the nucleus (reviewed in Xu and Massagué, 2004), we wondered whether FRA1 expression is decreased in the imb4 mutants. However, quantitative real-time PCR showed that FRA1 transcript levels were in fact higher in the imb4 mutants compared with wild-type plants (Figure 2A). In contrast, immunoblot analysis revealed that FRA1 protein level was greatly reduced in the imb4 mutants (Figure 2B). No such decrease was observed for β -tubulin and G-actin proteins in the *imb4* mutants, indicating that protein levels were not generally reduced (Figure 2B). Further, the fluorescence signal of FRA1-3GFP was greatly reduced in the imb4-1 fra1-5 double mutant compared with the fra1-5 background alone (Figure 2C), indicating that transgenically expressed FRA1-3GFP protein is also degraded in the imb4 mutants. In contrast, neither the amount nor localization of IMB4-tdTomato was affected in the fra1-5 mutant (Figures S3A-S3B). Notably, FRA1 protein levels were restored to normal in complemented imb4 mutants expressing either native promoter-driven IMB4-Myc or IMB4-tdTomato (Figure 2D).

Interestingly, we observed that IMB4-tdTomato protein levels in different regions of light-grown hypocotyls correlated with growth rate, similar to the FRA1 kinesin (Zhu et al., 2015). Specifically, rapidly elongating cells at the hypocotyl apex showed ~2.5-fold higher IMB4-tdTomato fluorescence signal compared with non-elongating cells at the hypocotyl base (Figure 2E). Therefore, the amount of IMB4 protein in a given cell appears to be developmentally regulated.

To define the pathway for FRA1 protein degradation, we performed a set of pharmacological experiments. When protein translation in wild-type seedlings was inhibited by cycloheximide, FRA1 protein levels decreased by \sim 60% after 16 hours (Figure 2F). Treatment with 100 μM of the 26S proteasome inhibitor MG132 (Abas et al., 2006) completely blocked the decrease in the amount of the FRA1 protein, whereas treatment with 50 μ M of the phosphatidylinositol 3-kinase inhibitor wortmannin, which inhibits membrane trafficking, including to the lytic vacuole (Kleine-Vehn et al., 2008), did not (Figures 2G and 2H). Correspondingly, treatment of the imb4 mutants with MG132 led to a 2-fold increase in FRA1 protein levels (Figures 2I and 2J). To further verify that the 26S proteasome is responsible for the degradation of FRA1, we probed steady-state FRA1 protein levels in three different A. thaliana proteasome mutants (rpn1a, rpt2a and rpn12) (Lee et al., 2011; Smalle et al., 2002;

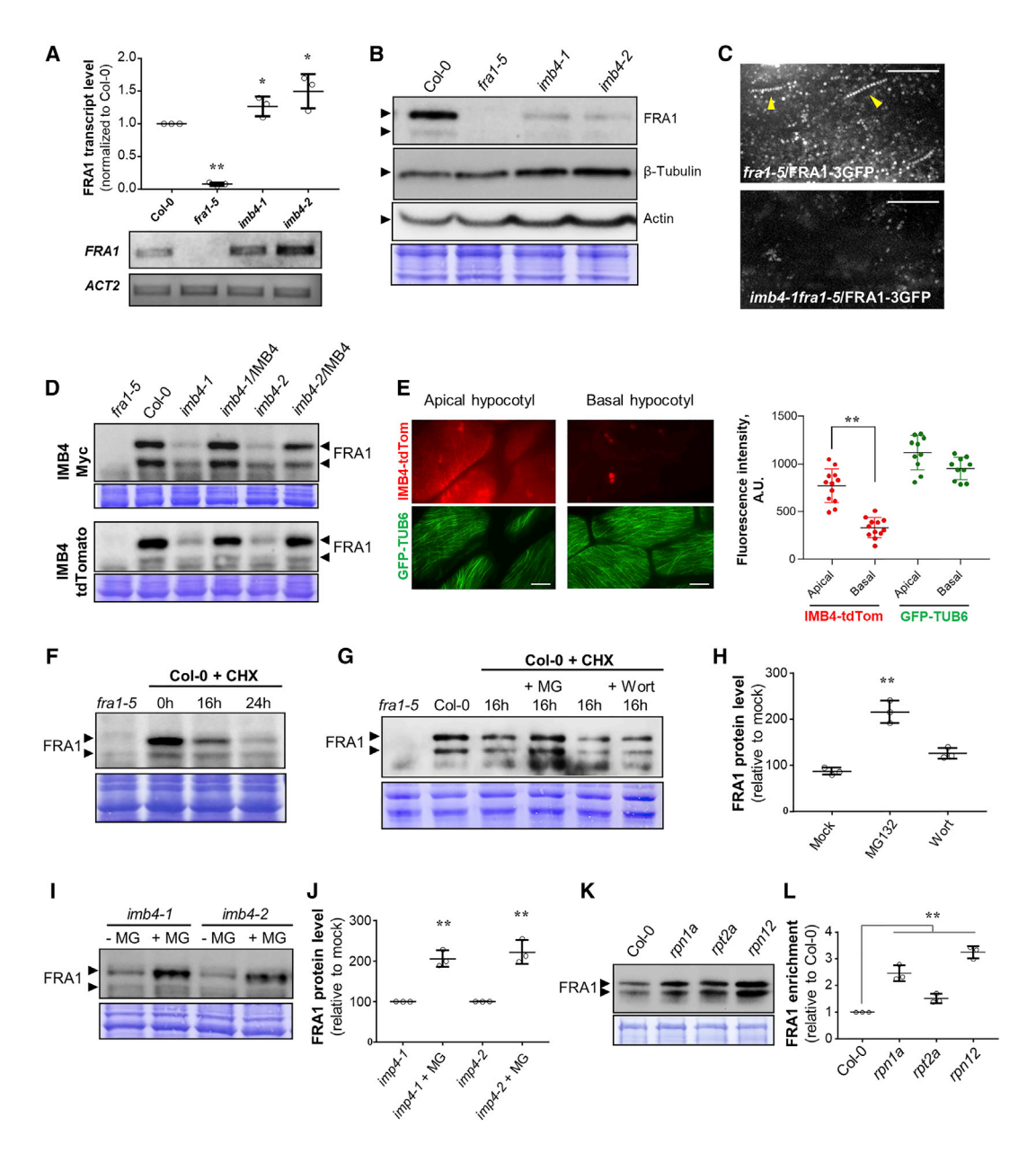


Figure 2. IMB4 Regulates FRA1 Protein Turnover by the 26S Proteasome

All data are for 5-day-old seedlings. The arrowheads in the immunoblots mark the expected positions of the respective proteins. The FRA1 protein frequently shows up as a doublet. Coomassie-stained gels are shown below each immunoblot as a loading control.

(A) FRA1 transcript levels determined by qRT-PCR. Values are means ± SEM from three biological replicates. The gel below shows FRA1 transcript levels by semi-qRT-PCR.

- (B) Immunoblot of total protein extracts probed with anti-FRA1, anti-β-tubulin, and anti-actin antibodies.
- (C) Time-projection images of FRA1-3GFP particles in fra1-5 and imb4-1fra1-5 mutants. The linear tracks (yellow arrowheads) represent motile events. Scale bar, 2 µm. (D) Immunoblots of total protein extracts probed with an anti-FRA1 antibody.
- (E) Micrographs of IMB4-tdTomato and GFP-TUB6 from cells in the apical and basal regions of the hypocotyl. The adjacent dot plot shows the fluorescence intensity at the cell cortex. Values are mean ± SD from 10 to 12 seedlings. Scale bar, 5 μm.
- (F) Total protein extracts from Col-0 plants treated with 50 µM cycloheximide (CHX) at 0-, 16-, and 24-hour time points probed with an anti-FRA1 antibody. (G and H) Immunoblotting and quantification of FRA1 protein levels with and without treatment with 100 μM MG132 (MG) and 50 μM wortmannin (Wort) in the presence of CHX for 16 hours. Values are means \pm SD (n = 3 replicates).
- (I and J) Immunoblotting and quantification of FRA1 protein levels with and without treatment with 100 µM MG132 in the presence of CHX for 16 hr. Values are means \pm SD (n = 3 replicates).

(K and L) Immunoblotting and quantification of FRA1 protein levels in three different 26S proteasome mutants relative to Col-0 control plants. Values are means ± SD (n = 3 replicates).

Asterisks indicate significant differences between the genotypes or between inhibitor treatments as determined by Student's t test, *p < 0.01, **p < 0.001. See also Figure S3.

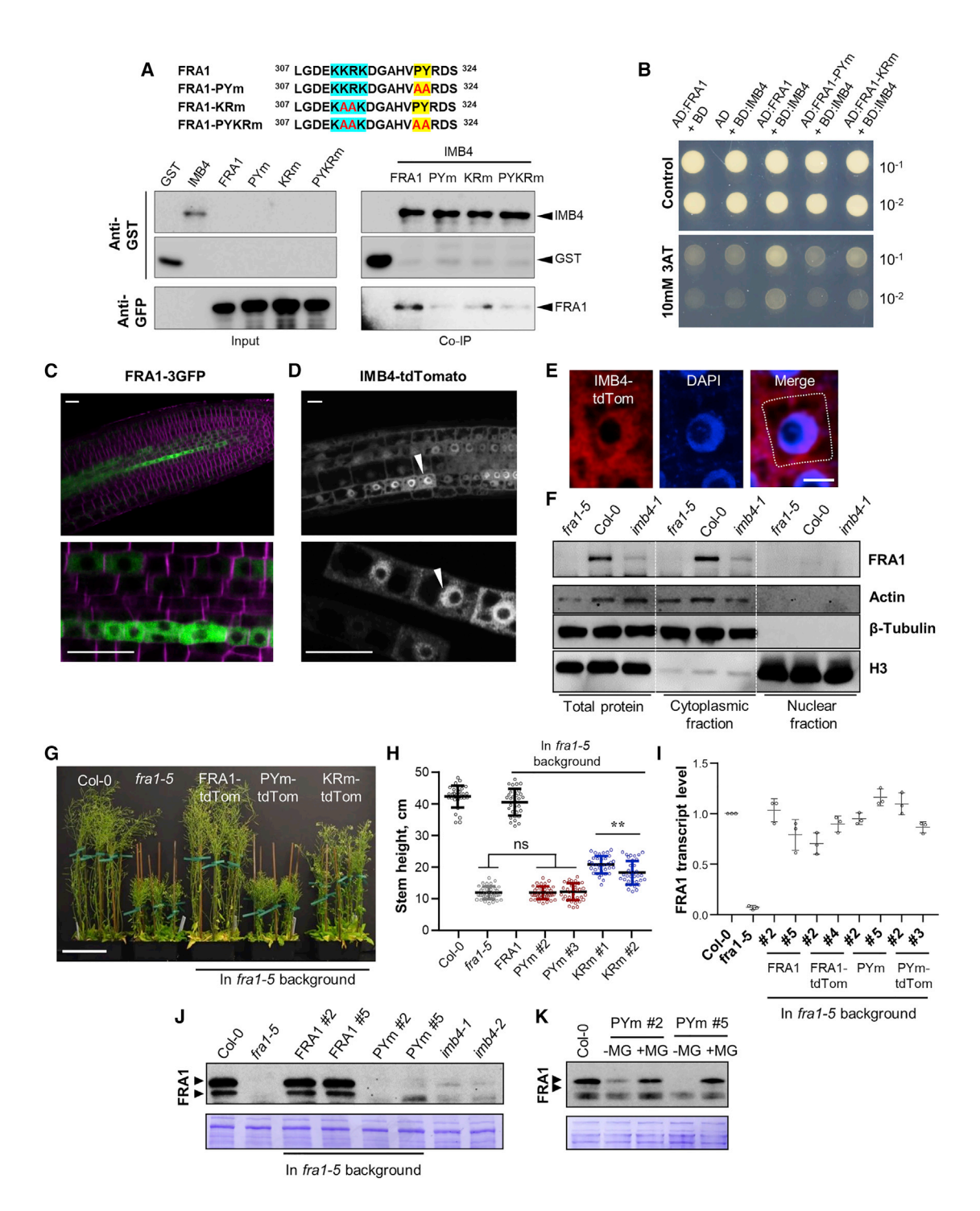


Figure 3. IMB4 Interacts with a PY Motif in the FRA1 Motor Domain

All immunoblots are representative of at least three independent experiments.

(A) The residues constituting a PY-NLS motif are highlighted in the FRA1 motor domain amino acid sequence. The immunoblot below shows a pull-down experiment with GST-IMB4 incubated with equal amounts of the indicated FRA1(707)-GFP motor domains. GST alone was used as a negative control. (B) Yeast two-hybrid assay using either the wild-type or PY-mutated FRA1 motor domain fused with the activation domain (AD) as prey and IMB4 fused with the DNA binding domain (BD) as bait.

(C) Confocal micrograph of FRA1-3GFP (green) in the root vasculature of a 4-day-old seedling. Cell boundaries in the root were visualized by staining with 5 μ M FM4-64 (magenta) for 10 min. A higher-magnification image is shown below. Scale bar, 10 μ m.

(D) Confocal micrograph of IMB4-tdTomato in the root epidermis of a 4-day-old seedling. A higher-magnification image is shown below. Arrowheads label nuclei. Scale bar, 10 μm .

Wang et al., 2009) using immunoblot analysis. All three mutants showed significantly increased FRA1 protein level (Figures 2K and 2L), thus confirming that FRA1 is degraded primarily by the proteasome system.

Consistent with our finding that FRA1 is degraded in the *imb4* mutants, we observed a 50% decrease in the secondary cell wall thickness and in the rate of pectin secretion in the *imb4* mutants (Figures S4A–S4D), similar to the *fra1-5* mutant (Zhu et al., 2015).

Binding of IMB4 to a PY Motif in the Motor Domain of FRA1 Prevents the Proteasome-Mediated Degradation of FRA1

To determine whether IMB4 directly protects FRA1 against degradation, we conducted structure-function studies to identify the IMB4-interaction motif in FRA1. Sequence analysis of the FRA1 protein revealed a proline-tyrosine nuclear localization sequence (NLS)-like motif in its motor domain (Figure 3A), which is recognized by karyopherin-β2 in mammals (Lee et al., 2006). To determine whether this motif mediates the FRA1-IMB4 interaction, we created two mutant versions of FRA1: one in which the PY residues were replaced with AA residues (PYm) and a second in which the basic KKRK motif was changed to KAAK (KRm). The PYm mutant showed significantly reduced IMB4 binding, whereas the KRm mutant showed only modestly decreased binding to IMB4, in pull-down and yeast two-hybrid interaction assays (Figures 3A and 3B). It is possible that mutation of all four basic residues might further decrease binding of FRA1 to IMB4.

Since metazoan importin-4β (IPO4/RanBP4/IMP4) mediates nuclear import of ribosomal proteins (Rout et al., 1997; Jäkel et al., 2002), we wondered whether IMB4 shuttles FRA1 into the nucleus. However, confocal imaging of a functional FRA1-3GFP fusion protein (Zhu et al., 2015) showed that FRA1-3GFP was localized predominantly in the cytoplasm (Figure 3C). In contrast, a functional full-length IMB4 labeled with tdTomato and expressed under the control of its native promoter in the imb4-1 mutant (Figures S3C and S3D) showed both cytosolic and nuclear localization (Figures 3D and 3E). To verify that the large 3GFP tag did not hamper nuclear import of FRA1, we isolated nuclei from fra1-5, imb4-1, and wild-type plants and used immunoblotting to determine whether the native FRA1 protein is present in the nuclear fraction. We found that FRA1 was almost entirely present in the cytoplasmic fraction (Figure 3F), consistent with our microscopy data. Therefore, we conclude that binding of IMB4 does not lead to translocation of FRA1 into the nucleus.

To determine the function of the PY motif-mediated interaction between FRA1 and IMB4, we introduced the PYm and KRm versions of full-length FRA1 into the fra1-5 background. The FRA1-PYm-expressing plants (both the untagged and the tdTomato-tagged versions) failed to complement the dwarf phenotype of the fra1-5 mutant, whereas the FRA1-KRm-expressing plants showed partial rescue (Figures 3G, 3H, S4E, and S4F). Transcript analysis showed that FRA1 mRNA levels in the FRA1-PYm plants were similar to those in wild-type and fra1-5 complemented plants (Figure 3I). In contrast, immunoblot analysis showed that the FRA1 protein levels in the FRA1-PYm plants were similar to the levels in the imb4 mutants (Figure 3J). Furthermore, the FRA1 protein levels in two independent FRA1-PYm lines were restored to wild-type levels after treatment with MG132 for 20 hr (Figure 3K). Together, these findings demonstrate that interaction of IMB4 with the PY motif protects FRA1 against proteasomemediated degradation.

Binding of IMB4 to the PY Motif Inhibits the Microtubule Interaction and Motility of FRA1

The PY motif is adjacent to highly conserved amino acids in the loop 12-helix α5 portion of the motor domain, which are part of the MT-binding interface of kinesins (Figure 4G) (Sawin et al., 1992; Woehlke et al., 1997). To determine whether binding of IMB4 to the PY motif inhibits the interaction of FRA1 to MTs, we performed MT co-sedimentation assays with FRA1(707)-GFP in the presence or absence of a truncated, more soluble version of IMB4 (Δ IMB4, amino acids 151-894) that also interacts with the FRA1 motor domain (Figure S4G). Both FRA1(707)-GFP and FRA1-PYm(707)-GFP associated with MTs in the presence and absence of the non-hydrolyzable ATP analog, AMPPNP, indicating that the PY residues do not function in MT binding (Figure 4A and 4B). Furthermore, Δ IMB4 by itself does not bind to MTs in vitro (Figure S4H), indicating that ΔIMB4 does not compete with FRA1 for MT-binding sites. However, addition of ΔIMB4 significantly decreased the binding of FRA1(707)-GFP, but not of FRA1-PYm(707)-GFP, to MTs (Figure 4A-4C), demonstrating that binding of IMB4 to the PY motif directly inhibits the interaction of FRA1 with MTs. To determine the effect of IMB4 on the motility of FRA1(707)-GFP, we conducted in vitro singlemolecule motility assays with or without ΔIMB4. In control experiments, FRA1(707)-GFP molecules readily bound to MTs and showed extensive processive motility (Figures 4D, S4I, and S4J). In contrast, both MT binding and motility of FRA1 were reduced by almost 3-fold when IMB4 was included in the motility mix (Figures 4E, 4F, S4I, and S4J), providing clear

⁽E) The nuclear signal of IMB4-tdTomato (red) colocalizes with DAPI (blue) signal in root cells. The dashed line in the merged image marks the cell boundary. Scale bar, 5 μm.

⁽F) Immunoblots of total, cytoplasmic, and nuclear fractions isolated from 5-day-old *fra1-5*, Col-0, and *imb4-1* seedlings. The purity of the cytoplasmic and nuclear fractions was determined by blotting with anti-actin, anti-β-tubulin, and anti-histone H3 antibodies, respectively.

⁽G and H) Whole-plant morphology and primary inflorescence stem heights of 40-day-old plants grown in continuous light. Values are means ± SD (n = 30 plants). Scale bar, 10 cm.

⁽I) FRA1 transcript levels relative to wild-type (Col-0) plants determined by qRT-PCR. Values are means ± SEM from three biological replicates.

⁽J) Immunoblot of total protein extracts probed with an anti-FRA1 antibody. The FRA1 protein level in two independent FRA1-PYm lines is consistently similar to the fra1-5 and imb4 mutants.

⁽K) Immunoblot analysis of the FRA1 protein in two independent *fra1-5/FRA1-PYm* lines with or without treatment with 50 μM MG132 for 24 hr. Asterisks indicate significant difference compared with *fra1-5* as determined by Student's t test, **p < 0.001. See also Figure S4.

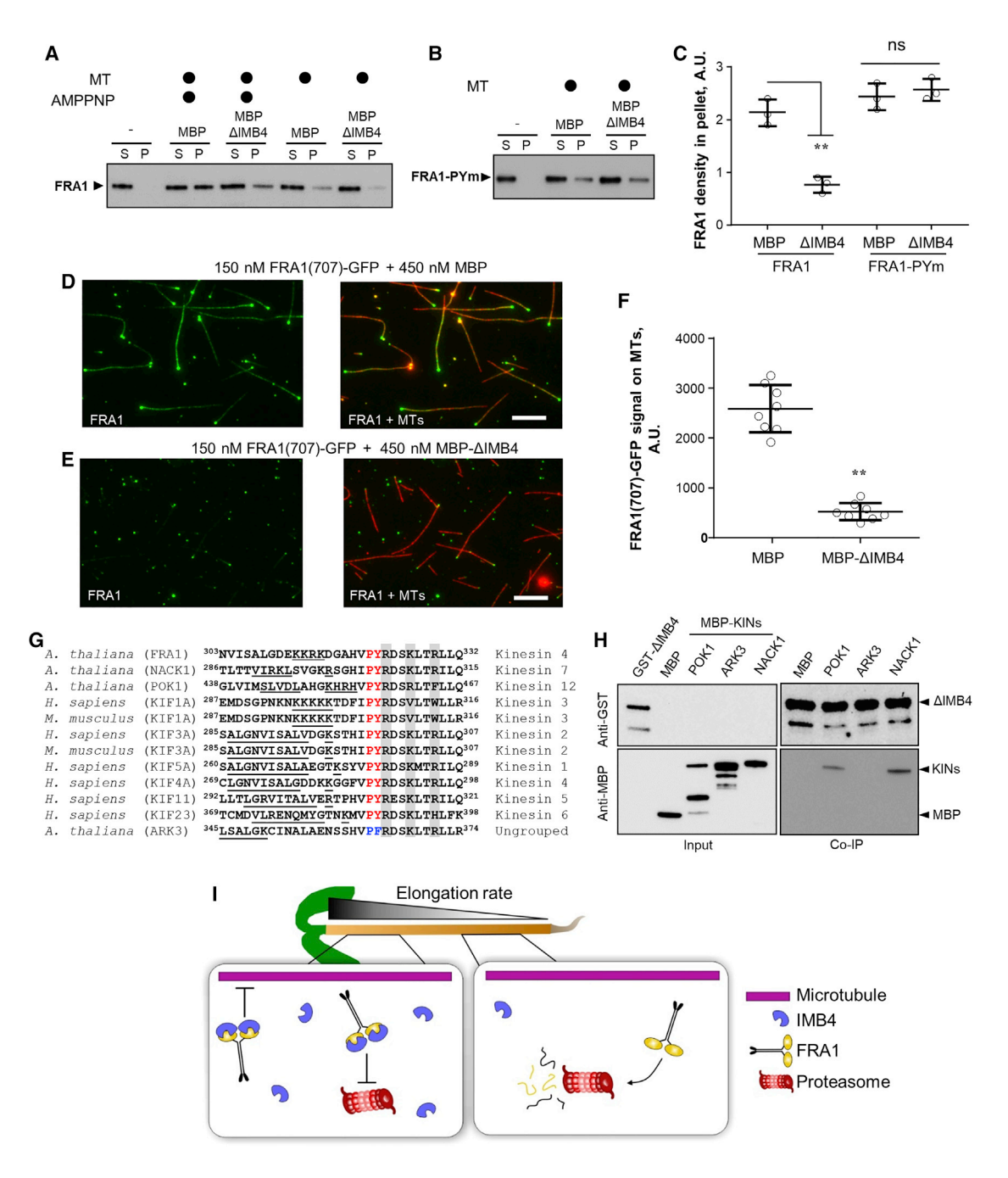


Figure 4. Binding of IMB4 to the Motor Domain Inhibits FRA1 Motility

All immunoblots are representative of at least three independent experiments.

(A and B) MT co-sedimentation assays with FRA1(707)-GFP (FRA1) and FRA1(707)-GFP-PYm (FRA1-PYm) proteins in the presence of MBP-ΔIMB4. MBP is used as a negative control. S, supernatant; P, pellet.

(C) Quantification of the FRA1 and FRA1-PYm protein levels in the pellet fractions from experiments shown in (A) and (B). Values are means ± SD. **p < 0.001. ns, not significant.

(D and E) Fluorescence micrographs of in vitro motility assays with 150 nM FRA1(707)-GFP and rhodamine-labeled MTs in the presence of 450 nM MBP or MBP-ΔIMB4, respectively. Scale bars, 5 μm.

(F) Quantification of the FRA1(707)-GFP fluorescence signal on MTs from experiments shown in (D) and (E). Values are means ± SD. Asterisks indicate significant differences as determined by Student's t test, **p < 0.001.

(G) Alignment of amino acid sequences within the motor domain of select kinesins from Arabidopsis and mammals. The consensus sequences that are thought to define a PY motif are the PY residues (red) and either basic or hydrophobic residues preceding the PY (underlined). Residues highlighted in gray are known to be critical for binding to microtubules. The Arabidopsis ARK3 kinesin does not contain a canonical PY motif (blue).

(H) In vitro pull-down assay with GST-ΔIMB4 and the motor domains of the Arabidopsis POK1, NACK1, and ARK3 kinesins.

(legend continued on next page)

evidence for the inhibitory effect of IMB4 on the MT association and motility of FRA1.

IMB4 Directly Interacts with Plant Mitotic Kinesins

The PY motif exists in the motor domains of diverse kinesin families in both plants and animals (Figure 4G). To examine whether it mediates binding of IMB4 to other Arabidopsis kinesins, we selected the Phragmoplast Orienting Kinesin 1, POK1 (At3g17360) (Muller et al., 2006), and the NPK1-Activating Kinesin 1, NACK1 (At1g18370) (Nishihama et al., 2002), as candidates that contain the PY motif in their motor domains (Figure 4G). Both POK1 and NACK1 motor domains showed direct interaction with IMB4 in pull-down experiments (Figure 4H). In contrast, another kinesin from an ungrouped family, ARK3 (At1g12430) (Sakai et al., 2008), which does not contain a PY motif in its motor domain, failed to show detectable interaction with IMB4 (Figure 4H). These data suggest that regulation of kinesins by the binding of importin-β to the PY motif in the motor domain is likely to be a common mechanism across multiple kinesin families.

DISCUSSION

Cells control the motility of kinesins to ensure that they are active only when needed (reviewed in Ganguly and Dixit, 2013; Lee et al., 2015; Verhey and Hammond, 2009). In plants, FRA1 levels correlate with growth rate, suggesting that FRA1 is engaged only when there is a need for high-capacity cell wall secretion. Here, we show that direct interaction of IMB4 with a PY motif in the motor domain of FRA1 regulates both the motility and abundance of FRA1. IMB4 directly prevents the motor domain of FRA1 from binding to MTs, thereby keeping FRA1 in an inactive state. In addition, IMB4 binding inhibits the degradation of FRA1 by the proteasome system. Based on these data, we propose a model for how plants developmentally regulate the motility and lifetime of FRA1 molecules in cells that produce primary cell walls. In rapidly growing cells, binding of IMB4 keeps FRA1 inactive but also resistant to degradation, which works to maintain a high pool of FRA1 in the cytoplasm (Figure 4I). When growth slows, IMB4 levels decline, in turn making FRA1 susceptible to the proteasome system and hence decreasing the amount of FRA1 when the demand for cell wall material diminishes (Figure 4I).

Our data suggest that IMB4 directly blocks the MT-binding interface of the FRA1 motor domain, similar to the inhibitory mechanism proposed by the binding of importin- α to a monopartite NLS within the motor domain of the MT, depolymerizing kinesin-13 kif2a (Wilbur and Heald, 2013). We expect the PY motif-based regulatory mechanism to be widespread based on the presence of this motif in the motor domains of multiple kinesin families in plants and animals. We found that two *Arabidopsis* mitotic kinesins that contain PY motifs in their motor domains, the kinesin-12 POK1 and the kinesin-7 NACK1, interact directly with IMB4. The presence of abnormal cell division planes in the

roots of *imb4* mutants, which resemble the cytokinetic defects in the *pok1* and *nack1* mutants (Muller et al., 2006; Nishihama et al., 2002), suggest that IMB4 might regulate POK1 and NACK1 kinesins during cytokinesis. It will be interesting to determine whether importins also bind to the PY motif of mammalian kinesins and regulate their motility.

In metazoa, binding of importin- α/β can regulate the subcellular localization of kinesins. Binding of importin- α/β to the mitotic kinesin-14 XCTK2 leads to sequestration of XCTK2 in the nucleus during interphase (Cai et al., 2009; Ems-McClung et al., 2004; Weaver et al., 2015). Similarly, direct interaction of importin- β with a ciliary localization sequence in the tail domain of the kinesin-2 KIF17 leads to transport of KIF17 into the ciliary compartment (Dishinger et al., 2010). In contrast, interaction of IMB4 with FRA1 does not lead to significant steady-state accumulation of FRA1 in the nucleus.

The mechanism that causes IMB4 to dissociate from the motor domain to enable FRA1 motility remains unknown. A high concentration of RanGTP is known to activate kinesins by causing the dissociation of bound importin-α/β (Tahara et al., 2008; Trieselmann et al., 2003; Weaver et al., 2015). Although IMB4 interacts with the Arabidopsis Ran 1 (Figure S4K), whether plant cells generate RanGTP in the cytoplasm similar to the local production of RanGTP in nerve axons (Rishal and Fainzilber, 2014; Schulze et al., 2008; Yudin et al., 2008) remains to be determined. Alternatively, other mechanisms, such as phosphorylation or binding of regulatory proteins, might cause the release of IMB4 and activate FRA1. Collectively, our data reveal how the lifetime, MT-binding capacity, and motility of the FRA1 kinesin are regulated by IMB4 during cell wall biogenesis, shedding light on the mechanisms by which kinesins are regulated to perform their functions in eukaryotic cells.

STAR*METHODS

Detailed methods are provided in the online version of this paper and include the following:

- KEY RESOURCES TABLE
- CONTACT FOR REAGENT AND RESOURCE SHARING
- EXPERIMENTAL MODEL AND SUBJECT DETAILS
 - Plant Maintenance
- METHOD DETAILS
 - $\bigcirc \ \ \text{Yeast Two-Hybrid Assay}$
 - Bacterial Expression System
 - In Vitro Pull-Down Experiments
 - In Vivo Immunoprecipitation
 - Generation of Constructs for Transgenic Plants
 - O Variable Angle Epifluorescence Microscopy
 - Laser Scanning Confocal Microscopy
 - O Metabolic Labeling of Pectin Using Fucose-Alkyne
 - Quantitative RT-PCR and Immunoblotting of FRA1
 - Nuclear Isolation
 - In Vitro Microtubule Co-Sedimentation Assay

⁽I) Model for the developmental regulation of FRA1 by IMB4. In rapidly elongating cells, IMB4 protein levels are high and binding to the FRA1 motor domain prevents proteasome-mediated degradation of FRA1 and also inhibits its motility, thus maintaining a high level of FRA1 kinesin. When cell elongation ceases, IMB4 levels decline, thereby resulting in the rapid degradation of FRA1 by the proteasome.

See also Figure S4.

- In Vitro Motility Assay
- Transmission Electron Microscopy
- QUANTIFICATION AND STATISTICAL ANALYSIS
 - Analysis of FRA1 Motility

SUPPLEMENTAL INFORMATION

Supplemental Information includes four figures and one table and can be found with this article online at https://doi.org/10.1016/j.devcel.2018.01.027.

ACKNOWLEDGMENTS

We thank Richard Vierstra (Washington University in St. Louis) for kindly providing us with the anti-Histone3 antibody and the *Arabidopsis* proteasome mutants. We also thank Howard Berg (Donald Danforth Plant Science Center) for the electron microscopy of cell walls. This work was supported by the Monsanto/Norman Borlaug Corporate Fellowship to C.Z.; the Center for Lignocellulose Structure and Formation, an Energy Frontier Research Center funded by the U.S. Department of Energy, Office of Science, Basic Energy Sciences (award DE–SC0001090) to the laboratory of C.T.A.; and the National Science Foundation (award MCB–1121287 and the Center for Engineering Mechanobiology, award CMMI-1548571) to the laboratory of R.D.

AUTHOR CONTRIBUTIONS

A.G. and R.D. conceptualized the project. R.D., C.T.A., A.G., and D.D.M. designed the research. A.G., L.D., C.Z., and D.D.M. performed the research. R.D., A.G., L.D., C.Z., and D.D.M. analyzed the data. A.G., R.D., and C.T.A. wrote the article. All authors read and approved the final version of the manuscript.

DECLARATION OF INTERESTS

The authors declare no competing financial interests.

Received: July 9, 2017 Revised: November 10, 2017 Accepted: January 29, 2018 Published: March 1, 2018

REFERENCES

Anderson, C.T., Wallace, I.S., and Somerville, C.R. (2012). Metabolic click-labeling with a fucose analog reveals pectin delivery, architecture, and dynamics in *Arabidopsis* cell walls. Proc. Natl. Acad. Sci. USA 109, 1329–1334.

Anderson, C.T., and Wallace, I.S. (2012). Illuminating the wall: using click chemistry to image pectins in *Arabidopsis* cell walls. Plant Signal. Behav. 7, 661–663.

Abas, L., Benjamins, R., Malenica, N., Paciorek, T., Wisniewska, J., Moulinier-Anzola, J.C., Sieberer, T., Friml, J., and Luschnig, C. (2006). Intracellular trafficking and proteolysis of the *Arabidopsis* auxin-efflux facilitator PIN2 are involved in root gravitropism. Nat. Cell Biol. 8, 249–256.

Blasius, T.L., Cai, D., Jih, G.T., Toret, C.P., and Verhey, K.J. (2007). Two binding partners cooperate to activate the molecular motor Kinesin-1. J. Cell Biol. *176*, 11–17.

Cahu, J., Olichon, A., Hentrich, C., Schek, H., Drinjakovic, J., Zhang, C., Doherty-Kirby, A., Lajoie, G., and Surrey, T. (2008). Phosphorylation by Cdk1 increases the binding of Eg5 to microtubules in vitro and in *Xenopus* egg extract spindles. PLoS One *3*, e3936.

Cai, D., Verhey, K.J., and Meyhofer, E. (2007a). Tracking single Kinesin molecules in the cytoplasm of mammalian cells. Biophys. J. 92, 4137–4144.

Cai, D., Hoppe, A.D., Swanson, J.A., and Verhey, K.J. (2007b). Kinesin-1 structural organization and conformational changes revealed by FRET stoichiometry in live cells. J. Cell Biol. *176*, 51–63.

Cai, S., Weaver, L.N., Ems-McClung, S.C., and Walczak, C.E. (2009). Kinesin-14 family proteins HSET/XCTK2 control spindle length by cross-linking and sliding microtubules. Mol. Biol. Cell 20, 1348–1359.

Coy, D.L., Hancock, W.O., Wagenbach, M., and Howard, J. (1999). Kinesin's tail domain is an inhibitory regulator of the motor domain. Nat. Cell Biol. 1, 288–292

Dietrich, K.A., Sindelar, C.V., Brewer, P.D., Downing, K.H., Cremo, C.R., and Rice, S.E. (2008). The kinesin-1 motor protein is regulated by a direct interaction of its head and tail. Proc. Natl. Acad. Sci. USA 105, 8938–8943.

Dishinger, J.F., Kee, H.L., Jenkins, P.M., Fan, S., Hurd, T.W., Hammond, J.W., Truong, Y.N., Margolis, B., Martens, J.R., and Verhey, K.J. (2010). Ciliary entry of the kinesin-2 motor KIF17 is regulated by importin-beta2 and RanGTP. Nat. Cell Biol. *12*, 703–710.

Ems-McClung, S.C., Zheng, Y., and Walczak, C.E. (2004). Importin alpha/beta and Ran-GTP regulate XCTK2 microtubule binding through a bipartite nuclear localization signal. Mol. Biol. Cell 15, 46–57.

Espeut, J., Gaussen, A., Bieling, P., Morin, V., Prieto, S., Fesquet, D., Surrey, T., and Abrieu, A. (2008). Phosphorylation relieves autoinhibition of the kinetochore motor Cenp-E. Mol. Cell *29*, 637–643.

Friedman, D.S., and Vale, R.D. (1999). Single-molecule analysis of kinesin motility reveals regulation by the cargo-binding tail domain. Nat. Cell Biol. 1, 293–297.

Funabiki, H., and Murray, A.W. (2000). The *Xenopus* chromokinesin Xkid is essential for metaphase chromosome alignment and must be degraded to allow anaphase chromosome movement. Cell *102*, 411–424.

Ganguly, A., DeMott, L., and Dixit, R. (2017). The *Arabidopsis* kinesin-4, FRA1, requires a high level of processive motility to function correctly. J. Cell Sci. *130*, 1232–1238.

Ganguly, A., and Dixit, R. (2013). Mechanisms for regulation of plant kinesins. Curr. Opin. Plant Biol. *16*, 704–709.

Gordon, D.M., and Roof, D.M. (2001). Degradation of the kinesin Kip1p at anaphase onset is mediated by the anaphase-promoting complex and Cdc20p. Proc. Natl. Acad. Sci. USA 98, 12515–12520.

Hackney, D.D., Baek, N., and Snyder, A.C. (2009). Half-site inhibition of dimeric kinesin head domains by monomeric tail domains. Biochemistry 48, 3448–3456.

Hammond, J.W., Blasius, T.L., Soppina, V., Cai, D., and Verhey, K.J. (2010). Autoinhibition of the kinesin-2 motor KIF17 via dual intramolecular mechanisms. J. Cell Biol. *189*, 1013–1025.

Hammond, J.W., Cai, D.W., Blasius, T.L., Li, Z., Jiang, Y.Y., Jih, G.T., Meyhofer, E., and Verhey, K.J. (2009). Mammalian kinesin-3 motors are dimeric in vivo and move by processive motility upon release of autoinhibition. PLoS Biol. 7, 650–663.

Hildebrandt, E.R., and Hoyt, M.A. (2001). Cell cycle-dependent degradation of the *Saccharomyces cerevisiae* spindle motor Cin8p requires APC(Cdh1) and a bipartite destruction sequence. Mol. Biol. Cell *12*, 3402–3416.

Imanishi, M., Endres, N.F., Gennerich, A., and Vale, R.D. (2006). Autoinhibition regulates the motility of the *C. elegans* intraflagellar transport motor OSM-3. J. Cell Biol. *174*, 931–937.

Jäkel, S., Mingot, J.-M., Schwarzmaier, P., Hartmann, E., and Görlich, D. (2002). Importins fulfil a dual function as nuclear import receptors and cytoplasmic chaperones for exposed basic domains. EMBO J. 21, 377–386.

Kleine-Vehn, J., Leitner, J., Zwiewka, M., Sauer, M., Abas, L., Luschnig, C., and Friml, J. (2008). Differential degradation of PIN2 auxin efflux Carrier by retromer-dependent vacuolar targeting. Proc. Natl. Acad. Sci. USA *105*, 17812–17817.

Kong, Z., Ioki, M., Braybrook, S., Li, S., Ye, Z.H., Julie Lee, Y.R., Hotta, T., Chang, A., Tian, J., Wang, G., et al. (2015). Kinesin-4 functions in vesicular transport on cortical microtubules and regulates cell wall mechanics during cell elongation in plants. Mol. Plant 8, 1011–1023.

Lee, B.J., Cansizoglu, A.E., Suel, K.E., Louis, T.H., Zhang, Z.C., and Chook, Y.M. (2006). Rules for nuclear localization sequence recognition by karyopherin beta 2. Cell *126*, 543–558.

Lee, K.H., Minami, A., Marshall, R.S., Book, A.J., Farmer, L.M., Walker, J.M., and Vierstra, R.D. (2011). The RPT2 subunit of the 26S proteasome directs complex assembly, histone dynamics, and gametophyte and sporophyte development in Arabidopsis. Plant Cell 23, 4298-4317.

Lee, Y.R.J., Qiu, W.H., and Liu, B. (2015). Kinesin motors in plants: from subcellular dynamics to motility regulation. Curr. Opin. Plant Biol. 28, 120-126.

Malcos, J.L., and Cyr, R.J. (2011). An ungrouped plant kinesin accumulates at the preprophase band in a cell cycle-dependent manner. Cytoskeleton 68, 247-258

Muller, S., Han, S., and Smith, L.G. (2006). Two kinesins are involved in the spatial control of cytokinesis in Arabidopsis thaliana. Curr. Biol. 16, 888-894. Nishihama, R., Soyano, T., Ishikawa, M., Araki, S., Tanaka, H., Asada, T., Irie, K., Ito, M., Terada, M., Banno, H., et al. (2002). Expansion of the cell plate in plant cytokinesis requires a kinesin-like protein/MAPKKK complex. Cell 109.87-99.

Rishal, I., and Fainzilber, M. (2014). Axon-soma communication in neuronal injury. Nat. Rev. Neurosci. 15, 32-42.

Rout, M.P., Blobel, G., and Aitchison, J.D. (1997). A distinct nuclear import pathway used by ribosomal proteins. Cell 89, 715-725.

Sakai, T., Honing, H., Nishioka, M., Uehara, Y., Takahashi, M., Fujisawa, N., Saji, K., Seki, M., Shinozaki, K., Jones, M.A., et al. (2008). Armadillo repeatcontaining kinesins and a NIMA-related kinase are required for epidermalcell morphogenesis in Arabidopsis. Plant J. 53, 157-171.

Sawin, K.E., Mitchison, T.J., and Wordeman, L.G. (1992). Evidence for kinesinrelated proteins in the mitotic apparatus using peptide antibodies. J. Cell Sci. 101. 303-313.

Schindelin, J., Arganda-Carreras, I., Frise, E., Kaynig, V., Longair, M., Pietzsch, S., Rueden, C., Saalfeld, S., Schmid, B., Tinevez, J.Y., et al. (2012). Fiji: an open-source platform for biological-image analysis. Nat. Methods 9, 676–682.

Schulze, H., Dose, M., Korpal, M., Meyer, I., Italiano, J.E., Jr., and Shivdasani, R.A. (2008). RanBP10 is a cytoplasmic quanine nucleotide exchange factor that modulates noncentrosomal microtubules. J. Biol. Chem. 283, 14109-14119

Senese, S., Cheung, K., Lo, Y.C., Gholkar, A.A., Xia, X., Wohlschlegel, J.A., and Torres, J.Z. (2015). A unique insertion in STARD9's motor domain regulates its stability. Mol. Biol. Cell 26, 440-452.

Smalle, J., Kurepa, J., Yang, P., Babiychuk, E., Kushnir, S., Durski, A., and Vierstra, R.D. (2002). Cytokinin growth responses in Arabidopsis involve the 26S proteasome subunit RPN12. Plant Cell 14, 17-32.

Sun, F., Zhu, C., Dixit, R., and Cavalli, V. (2011), Sunday Driver/JIP3 binds kinesin heavy chain directly and enhances its motility. EMBO J. 30, 3416-3429.

Tahara, K., Takagi, M., Ohsugi, M., Sone, T., Nishiumi, F., Maeshima, K., Horiuchi, Y., Tokai-Nishizumi, N., Imamoto, F., Yamamoto, T., et al. (2008). Importin-beta and the small guanosine triphosphatase Ran mediate chromosome loading of the human chromokinesin Kid. J. Cell Biol. 180, 493-506.

Tamura, K., and Hara-Nishimura, I. (2014). Functional insights of nucleocytoplasmic transport in plants. Front. Plant Sci. 5, 118.

Trieselmann, N., Armstrong, S., Rauw, J., and Wilde, A. (2003). Ran modulates spindle assembly by regulating a subset of TPX2 and Kid activities including Aurora A activation, J. Cell Sci. 116, 4791-4798.

Verhey, K.J., and Hammond, J.W. (2009). Traffic control: regulation of kinesin motors. Nat. Rev. Mol. Cell Biol. 10, 765-777.

Verhey, K.J., Lizotte, D.L., Abramson, T., Barenboim, L., Schnapp, B.J., and Rapoport, T.A. (1998). Light chain-dependent regulation of Kinesin's interaction with microtubules. J. Cell Biol. 143, 1053-1066.

Wang, S., Kurepa, J., and Smalle, J.A. (2009). The Arabidopsis 26S proteasome subunit RPN1a is required for optimal plant growth and stress responses. Plant Cell Physiol. 50, 1721-1725.

Weaver, L.N., Ems-McClung, S.C., Chen, S.H., Yang, G., Shaw, S.L., and Walczak, C.E. (2015). The Ran-GTP gradient spatially regulates XCTK2 in the spindle. Curr. Biol. 25, 1509-1514.

Wilbur, J.D., and Heald, R. (2013). Mitotic spindle scaling during Xenopus development by kif2a and importin α . Elife 2, e00290.

Woehlke, G., Ruby, A.K., Hart, C.L., Ly, B., Hom-Booher, N., and Vale, R.D. (1997). Microtubule interaction site of the kinesin motor. Cell 90, 207-216.

Xu, F., Xu, S., Wiermer, M., Zhang, Y., and Li, X. (2012). The cyclin L homolog MOS12 and the MOS4-associated complex are required for the proper splicing of plant resistance genes. Plant J. 70, 916-928.

Xu, L., and Massagué, J. (2004). Nucleocytoplasmic shuttling of signal transducers. Nat. Rev. Mol. Cell Biol. 5, 209-219.

Yudin, D., Hanz, S., Yoo, S., Iavnilovitch, E., Willis, D., Gradus, T., Vuppalanchi, D., Segal-Ruder, Y., Ben-Yaakov, K., Hieda, M., et al. (2008). Localized regulation of axonal RanGTPase controls retrograde injury signaling in peripheral nerve. Neuron 59, 241-252.

Zhong, R., Burk, D.H., Morrison, W.H., 3rd, and Ye, Z.H. (2002). A kinesin-like protein is essential for oriented deposition of cellulose microfibrils and cell wall strength. Plant Cell 14, 3101-3117.

Zhu, C., and Dixit, R. (2011). Single molecule analysis of the Arabidopsis FRA1 kinesin shows that it is a functional motor protein with unusually high processivity. Mol. Plant 4, 879-885.

Zhu, C., Ganguly, A., Baskin, T.I., McClosky, D.D., Anderson, C.T., Foster, C., Meunier, K.A., Okamoto, R., Berg, H., and Dixit, R. (2015). The Fragile Fiber1 kinesin contributes to cortical microtubule-mediated trafficking of cell wall components. Plant Physiol. 167, 780-792.



STAR***METHODS**

KEY RESOURCES TABLE

REAGENT or RESOURCE	SOURCE	IDENTIFIER
Antibodies		
Rabbit polyclonal anti-FRA1	Zhu et al., 2015	N/A
Mouse monoclonal anti-GST	ThermoFisher	Cat# MA4-004; RRID: AB_10979611
Mouse monoclonal anti-tubulin-beta	Sigma	Cat# T4026; RRID: AB_477577
Mouse monoclonal anti-MBP	DSHB	Cat# DSHB-MBP-2A1; RRID: AB_2617428
Mouse monoclonal anti-GFP	Clontech	Cat# 632381; RRID: AB_2313808
Mouse monoclonal anti-Actin	DSHB	Cat# JLA20; RRID: AB_528068
Rabbit polyclonal anti-Histone H3	Abcam	Cat# ab1791; RRID: AB_302613
Rabbit polyclonal anti-Mouse IgG-HRP	Jackson Immuno Research	Cat# 715-035-151; RRID: AB_2340771
Donkey polyclonal anti-Rabbit IgG-HRP	Jackson Immuno Research	Cat# 711-035-152; RRID: AB_10015282
Bacterial and Virus Strains		
Rosetta™(DE3) Competent Cells	EMD Millipore	Cat# 70954
BL21-CodonPlus(DE3)-RIPL cells	Agilent Technologies	Cat# 230280
Biological Samples		
SALK_049564 (imb4-1)	ABRC	http://abrc.osu.edu
SAIL_155b-F06 (imb4-2)	ABRC	http://abrc.osu.edu
fra1-5	Zhu et al., 2015	N/A
Chemicals, Peptides, and Recombinant Proteins		
Z-Leu-Leu-Leu-al (MG132)	Sigma-Aldrich	Cat# C2211
Wortmannin	Sigma-Aldrich	Cat# W1628
Isopropyl-β-D-thiogalactoside	Sigma-Aldrich	Cat# 11411446001
3-Amino-1,2,4-triazole (3AT)	Sigma-Aldrich	Cat# A8056
Pierce protease inhibitor tablets	ThermoFisher	Cat# 88266
Phenylmethanesulfonyl fluoride (PMSF)	Sigma-Aldrich	Cat# P7626
4',6-diamidin-2-phenylindol (DAPI)	Sigma-Aldrich	Cat# D9542
FM4-64 (synaptored)	Tocris Bioscience	Cat# 5118
B-PER™ Bacterial Protein Extraction Reagent	ThermoFisher	Cat# 78248
Lysozyme from chicken egg white	Sigma-Aldrich	Cat# L6876
PVDF Membranes	ThermoFisher	Cat# 88518
SuperSignal™ West Dura Extended Duration Substrate	ThermoFisher	Cat# 34075
Tubulin protein (rhodamine): porcine brain	Cytoskeleton, Inc.	Cat# TL590M
Tubulin protein (>99% pure): porcine brain	Cytoskeleton, Inc.	Cat# T240
Paclitaxel (Taxol)	Cytoskeleton, Inc.	Cat# TXD01
Pectinase from Aspergillus niger	Sigma-Aldrich	Cat# P2736
KOD Hot Start DNA Polymerase	EMD Millipore	Cat# 71086
Ni-NTA Agarose	Qiagen	Cat# 30210
Amylose Resin	New England Biolabs	Cat# E8021S
Glutathione sepharose 4B	GE Healthcare	Cat# v17-0756-01
Anti-GFP mAb Agaraose	MBL International	Cat# D153-8
Gateway BP Clonase II Enzyme Mix	ThermoFisher	Cat# 11789100
LR Clonase II Plus enzyme	ThermoFisher	Cat# 12538200
pENTR11	Invitrogen	Cat# PQ1000101
pDEST22	Invitrogen	Cat# PQ1000101
pDEST32	Invitrogen	Cat# PQ1000101

(Continued on next page)

Continued			
REAGENT or RESOURCE	SOURCE	IDENTIFIER	
pGEX-6p-1 (GST tag)	GE Healthcare	Cat# 28-9546-48	
pMAL-C5X (MBP tag)	New England Biolabs	Cat# N8108S	
pTEV (6x His tag)	Zhu and Dixit, 2011	N/A	
Critical Commercial Assays			
Purelink Quick Plasmid Miniprep Kit	Invitrogen	Cat# K210010	
Purelink PCR Purification Kit	Invitrogen	Cat# K310001	
Purelink Quick Gel Extraction Kit	Invitrogen	Cat# K210012	
RevertAid First Strand cDNA Synthesis Kit	ThermoFisher	Cat# K1621	
Oligonucleotides			
Please see Table S1	N/A	N/A	
Recombinant DNA			
pGEX-6p-1:IMB4	This study	N/A	
pGEX-6p-1:ΔIMB4(151-894aa)	This study	N/A	
pMAL-C5X:IMB4	This study	N/A	
pMAL-C5X:ΔIMB4(151-894aa)	This study	N/A	
pENTR11:FRA1(1-530)	This study	N/A	
pDEST22: FRA1(1-530)	This study	N/A	
pENTR11:IMB4	This study	N/A	
pDEST32:IMB4	This study	N/A	
pTEV:FRA1(1-707aa)	Zhu and Dixit, 2011	N/A	
pMAL-C5X:NACK1(1-540aa)	This study	N/A	
pMAL-C5X:POK1(1-500aa)	This study	N/A	
pMAL-C5X:KINUA(1-512aa)	This study	N/A	
pCambia1300:ProFRA1:FRA1	This study	N/A	
pCambia1300:ProFRA1:FRA1:tdTOMATO	Zhu et al., 2015	N/A	
pCambia1300:ProFRA1:FRA1:3GFP	Zhu et al., 2015	N/A	
pCambia1300:ProIMB4:IMB4-Myc	This study	N/A	
pCambia1300:ProIMB4:IMB4-tdTOMATO	This study	N/A	
pCambia2300:ProCamv35S:IMB4-GFP	This study	N/A	
pCambia2300:ProCamv35S:GFP	This study	N/A	
Software and Algorithms			
ImageJ (Fiji)	Schindelin et al., 2012	http://fiji.sc/	
Slidebook 6	Intelligent Imaging Innovations	https://www.intelligent-imaging.com/slidebook	

CONTACT FOR REAGENT AND RESOURCE SHARING

Further information and requests for reagents and resources may be directed to and will be fulfilled by the Lead Contact, Ram Dixit (ramdixit@wustl.edu).

EXPERIMENTAL MODEL AND SUBJECT DETAILS

Plant Maintenance

Arabidopsis thaliana Col-0 plants were used for experiments. The fra1-5 mutant has been described previously (Zhu et al., 2015). The imb4-1 and imb4-2 mutants were isolated from T-DNA insertion lines (SALK_049564/imb4-1 and SAIL_155b-F06/imb4-2) obtained from the ABRC (http://abrc.osu.edu/). Homozygous mutants were identified by using primers listed in Table S1. For growth on plates, seeds were sterilized with 25% (v/v) bleach for 10 min, rinsed thrice with water and planted on 0.5X Murashige and Skoog medium (MS, Caisson Laboratories). Seeds were stratified at 4°C for 2-3 d and then germinated and grown at 23°C under 16 h of light. For dark grown seedlings, seedlings were pre-exposed to light for 4 h before being placed in dark at 22°C. Live imaging experiments used 4-d-old light-grown seedlings unless otherwise stated. For growth in soil, seeds were grown under continuous light, 70% humidity, and 22°C after stratification at 4°C for 2 d.



METHOD DETAILS

Yeast Two-Hybrid Assay

Directed yeast two-hybrid experiments were performed according to the ProQuest[™] Two-Hybrid System with Gateway® Technology manual (Invitrogen). Full-length IMB4 and the FRA1-motor domain (amino acids 1-530) were first cloned into the entry vector pENTR 11 with enzymes Kpn1 and Not1 for IMB4 and Kpn1 and EcoR1 for FRA1 (for primers, see Table S1). From the entry clones, IMB4 and FRA1-motor domain were then cloned into pDEST32 and pDEST22 vectors, respectively, using LR Clonase II enzyme (Invitrogen). These constructs together with all the controls were then transformed into the MaV203 Competent Yeast Cells (Saccharomyces cerevisiae) and selected on SD-Leu-Trp plates. For each set, at least four independent colonies were used for yeast two-hybrid assay on SD-Leu-Trp-His plates with and without 5-10 mM 3-AT (3-Amino-1,2,4-triazole) (Sigma). Colonies were imaged every 24 h post plating for 4-5 days.

Bacterial Expression System

For protein expression in *E. coli*, Rosetta (DE3) cells (EMD Millipore) and BL21-CodonPlus(DE3)-RIPL cells (Agilent) were used. Cells were induced with IPTG (Sigma) with concentrations between 0.1 to 0.5 mM at temperatures ranging between 16°C to 24°C. Coding sequences were cloned in pGEX-6p-1 (GST tag), pMAL-c5x (MBP tag) and a modified pET-28c called pTEV (6x-His tag) for bacterial expression with primers listed in Table S1.

In Vitro Pull-Down Experiments

IMB4 and \(\Delta IMB4 \) were cloned into both the pGEX-6p-3 and the pMAL:c5x vectors to obtain N-terminal GST- and MBP-tagged fusion proteins. The FRA1(707)-GFP motor domain construct has been described previously (Zhu and Dixit, 2011). NACK1(1-540aa), POK1(1-500aa) and KINUA(1-512aa) motor domains were also cloned in the pMAL:c5x vector to obtain N-terminal MBP-tagged fusion proteins. For the FRA1 mutant constructs, site-directed mutagenesis was performed by the megaprimer protocol using primers listed in Table S1. Plasmids were transformed into BL21-DE3-RIPL competent cells (Agilent) and were induced with 0.5 mM IPTG for 4 hours. Cells were lysed with Thermo Scientific Pierce B-PER Bacterial Protein Extraction Reagents (1 ml B-Per, 2 μl DNase1, 3 μl Lysozyme, 1X protease inhibitor, 1 mM PMSF). For the pull-down experiments, 40 μl of Glutathione Sepharose beads (GE healthcare) were first incubated with GST-IMB4, GST-∆IMB4 or GST alone (~5 ug each) at 4°C on a shaker (speed 10 rpm) for 4-6 h for binding. Then, purified FRA1 motor domain protein was added (\sim 5 μ g each) into the tubes and incubated for an additional 10-12 h as before. Subsequently, the beads were washed at least 5 times with 1X PBS + 0.1% (v/v/) Tween-20. For pull downs of MBP-tagged proteins, 20 ul of MBP-Trap agarose (Chromotek) was used. Proteins were isolated from the beads by adding 1X SDS loading dye, separated by SDS-PAGE and transferred to 0.45 μm PVDF membrane (Thermo Scientific). The blots were then probed with a monoclonal anti-GST antibody from Sigma (1:5,000), a monoclonal anti-GFP antibody from Fermentas (1:5,000) and a polyclonal anti-FRA1 antibody (1:2,000) described previously (Zhu et al., 2015). For secondary antibodies, anti-rabbit IgG HRP (1:10,000, Jackson Immuno Research) and anti-mouse IgG HRP (1:10,000, Jackson Immuno Research) were used. Detection was conducted using SuperSignal West Dura chemiluminescence substrate (Thermo Scientific).

In Vivo Immunoprecipitation

Cauliflower Mosaic Virus 35S promoter-driven GFP and IMB4-GFP constructs were introduced into the pCambia2300 vector using primers listed in Table S1. The constructs were transformed into Col-0 plants and homozygous transgenic plants were selected. For the immunoprecipitation assay, 7-day-old seedlings were homogenized in a mortar using lysis buffer (20 mM Hepes pH 7.5, 40 mM KCl, 1mM EDTA, 0.1% (v/v) Triton-X 100, 1X protease inhibitor cocktail, 1mM PMSF, 10% (v/v) glycerol). The homogenate was then centrifuged twice at 10,000 rpm for 10 min and incubated with 20 ul of anti-GFP agarose beads (MBL) for 12-16 h at 4°C on a rocking shaker. Beads were then washed at least 5 times with 1X PBS + 0.1% (v/v) Tween-20 solution. Proteins were isolated from the beads by adding 1X SDS loading dye, separated by SDS-PAGE and detected via immunoblotting as described in the previous section.

Generation of Constructs for Transgenic Plants

The pFRA1::FRA1-3GFP and pFRA1::FRA1-tdTomato constructs have been described in Zhu et al., 2015. The pFRA1:FRA1 (no tag) construct was generated by introducing the FRA1 cDNA into the pCAMBIA 1300 vector. For the FRA1 mutant constructs, site-directed mutagenesis was performed using the megaprimer protocol with primers listed in Table S1. The pIMB4::IMB4-tdTomato construct was generated using 2.3 kb sequence upstream of the IMB4 start codon and the full length IMB4 cDNA followed by tdTomato cDNA. For the pIMB4::IMB4-Myc construct, a single Myc tag was fused at the C-terminal end of the IMB4 cDNA. These constructs were ligated into the pCAMBIA 1300 and 2300 vectors and introduced into the imb4 mutants via Agrobacterium-mediated floral dip transformation. Transgenic plants were selected using 30 μg/mL hygromycin and homozygous lines expressing a single copy of the transgene were used for phenotypic analysis and imaging.

Variable Angle Epifluorescence Microscopy

Live imaging of FRA1-tdTomato, FRA1-3GFP and IMB4-tdTomato was conducted using variable-angle epifluorescence microscopy using a customized Olympus multi-color, multi-angle total internal reflection fluorescence system outfitted on an IX81 stand

equipped with a ZDC focal drift compensation module. Four-day-old seedlings were mounted in 0.5X MS media between two layers of double-sided adhesive tape. Unless otherwise stated, epidermal cells in the apical or sub-apical region of the hypocotyl were imaged. GFP and tdTomato were excited using 3 mW 488-nm and 5 mW 561-nm diode-pumped solid-state lasers (Melles Griot) and images were collected using 100X (NA 1.45) objective and back-illuminated electron-multiplying CCD camera (Hamamatsu, ImageEM) at 1-s intervals for single color imaging. For dual-channel imaging of FRA1-3GFP and IMB4-tdTomato, images were collected at 2-s intervals in the green and red channels. Bright, oval structures in live images are chloroplasts that are visible due to chlorophyll autofluorescence.

Laser Scanning Confocal Microscopy

A Nikon A1 laser scanning confocal microscope was used to study whether FRA1-3GFP and IMB4-tdTomato localized to the nucleus. For these experiments, FRA1-3GFP was imaged in the root vasculature, where its expression is high. IMB4-tdTomato expression was high in all tissues and we imaged both epidermal and vasculature cells with the same result. GFP was excited using 1 mW 488-nm laser (Melles Griot) and images were collected with a 40X or 60X lens (NA 1.3) and 500-550 nm emission filter set. For, FRA1-tdTomato and IMB4-tdTomato, tdTomato was excited using 2 mW 513-nm laser (Melles Griot) and images collected with a 40X or 60X lens (NA 1.3) and 575-600 nm emission filter set.

To image cell elongation and division phenotypes, seedlings were treated with 2 μ M FM4-64 for 10 min prior to imaging. Similarly, to stain nuclei, roots were treated with 2 μ g/ml of 4',6-diamidin-2-phenylindol (DAPI) in liquid MS media for 30 min followed by two washes with liquid media. Plants expressing *pFRA1::FRA1-3GFP* were crossed to the *imb4-1* mutant and F3 progeny homozygous for *FRA1-3GFP*, *fra1-5* and *imb4-1* were used for imaging.

Metabolic Labeling of Pectin Using Fucose-Alkyne

Fucose-alkyne-based labeling of pectin was conducted as described previously (Anderson et al., 2012). Briefly, 4-day-old light-grown seedlings in 0.5X MS liquid medium were incubated with 2.5 μ M fucose-alkyne for 4 hours during which the fucose-alkyne is taken up by cells and is primarily incorporated into a type of pectin called rhamnogalacturonan-I in the Golgi (Anderson et al., 2012; Anderson and Wallace, 2012). The alkynylated fucose-labeled pectin is then secreted to the cell wall, where it is click labeled for 1 hour using 0.1 μ M Alexa 488-azide, 1 mM CuSO₄, and 1 mM ascorbic acid. The root elongation and early differentiation zones of labeled seedlings were imaged with a Zeiss Cell Observer SD spinning disk confocal microscope (488 nm laser excitation, 525/25 emission filter) using a 63X 1.40 NA oil immersion objective. Z-stacks of epidermal cells were collected and cell wall-associated fluorescence intensity in maximum projections was measured using ImageJ, by calculating mean pixel intensity values for individual cells.

Quantitative RT-PCR and Immunoblotting of FRA1

Total RNA was extracted from 2-week old seedlings by the Trizol method. Complementary DNA (cDNA) was synthesized with revertAid First Strand cDNA Synthesis Kit (ThermoFisher Scientific) and qRT-PCR was performed using the SYBR method using primers listed in Zhu et al., 2015. ACTIN2 was used as a normalization control. Data were collected from three biological replicates.

For immunoblotting, proteins were isolated from 5-6 day old (unless otherwise mentioned), light-grown seedlings. Lysates were prepared by first grinding seedlings in liquid nitrogen and then homogenizing in protein isolation buffer (50 mM Tris-acetate, pH 7.5, 2 mM EDTA, 1 mM PMSF and protease inhibitor tablet from Roche). Total proteins (\sim 30 μ g each) were separated by SDS-PAGE, transferred to PVDF membrane (Thermo Scientific) and probed with anti-FRA1 primary antibody (1:1,000, Zhu et al., 2015) and anti-rabbit HRP secondary antibody (1:5,000, Jackson Immuno Research).

Nuclear Isolation

Isolation of nuclei from Arabidopsis seedlings was performed according to Xu et al., 2012. Total 2 gm of 6-day-old seedlings grown on 0.5X Murashige and Skoog medium were used for each genotype for the isolation of nuclei. Seedlings were collected, frozen in liquid nitrogen and homogenized into fine powder using a mortar and pestle. The powder was then gently dissolved in 5 ml ice cold lysis buffer by pipetting. The homogenate was filtered first through a 100 μ m and then a 40 μ m nylon mesh (samples were saved during each step as controls). The filtered homogenate was then centrifuged at 1,500 g at 4°C for 10 min to pellet the nuclei and the supernatant was saved as the cytoplasmic fraction. The nuclear fraction was then washed twice by gently re-suspending in 1 ml of nuclei resuspension buffer each time and centrifuging at 1,500 g at 4°C for 10 min. The washed nuclei were kept in nuclei storage buffer. Total protein, cytoplasmic and nuclear fractions were then analyzed using SDS-PAGE and immunoblotting with anti-actin, anti-histone H3 and anti-FRA1 antibody (see Key Resources Table).

In Vitro Microtubule Co-Sedimentation Assay

Microtubule co-sedimentation was performed in 50- μ l reactions containing 1 μ M FRA1(707)–GFP protein (either in presence or absence of 3 μ M of MBP and MBP- Δ IMB4 protein) with or without 4 μ M taxol-stabilized microtubules in BRB80 buffer containing 20 μ M taxol. The reaction mixture was incubated at 25°C for 20 min and then centrifuged at 20,000 g for 15 min to sediment microtubules. Supernatant and pellet fractions were then analyzed using SDS-PAGE and immunoblotting with anti-GFP antibody (JL-20, Fermentas) as described above.



In Vitro Motility Assay

Rhodamine-labeled microtubules were assembled using unlabeled tubulin and rhodamine-labeled tubulin at a ratio of 25:1. The in vitro motility experiments were conducted as described previously in Zhu and Dixit, 2011. Briefly, flow cells (20-µl volume) were constructed using glass slides and silanized coverslips that were attached with double-sided adhesive tape. The flow cell was coated with 0.2% monoclonal anti-tubulin antibody (clone Tub 2.1, Sigma) and then blocked with 5% (w/v) Pluronic F-127 (Sigma). Then, 1:100 diluted rhodamine-labeled microtubules in MAB buffer containing 20 µM taxol were introduced into the flow cell and the unbound microtubules were washed away by MAB buffer containing 20 µM taxol. Lastly, a motility mix containing 150 nM of FRA1(707)-GFP, 450 nM MBP or MBP-ΔIMB4, 1 mM ATP, 50 mM DTT and an oxygen-scavenging system consisting of 250 µg/ml glucose oxidase, 35 µg/ml catalase and 4.5 mg/ml glucose was flowed in. FRA1 was pre-incubated with either MBP or MBP-∆IMB4 for 10 min at room temperature (~24°C) before being added to the motility mix. Excitation was achieved using 488-nm and 561-nm diode-pumped solid-state lasers (Melles Griot) to visualize FRA1(707)-GFP and rhodamine-labeled microtubules, respectively. Images were collected with a 100X TIRF objective (NA 1.45) and back-illuminated electron-multiplying CCD camera (Hamamatsu, ImageEM) using time-lapse capture at 1-s intervals in the GFP channel.

Transmission Electron Microscopy

To image cell walls, freshly cut 1 mm cross sections of 5-week-old basal stems were fixed using freshly prepared 2% (w/v) glutaraldehyde buffered with 0.1M Pipes buffer, pH 6.8 for 90-120 min at room temperature. The tissues were then rinsed three times in Pipes buffer and postfixed in 2% (w/v) osmium tetroxide buffer for 90 min. Following three rinses in water, the specimens were dehydrated in an ethanol/acetone series consisting of 5%, 10%, 20%, 30%, 50%, 75%, and 95% (v/v) ethanol, 20 min each, then 30 min in 100% ethanol and finally in 100% acetone for 15 min and 45 min. Specimens were then infiltrated with Spurr's resin and thin sections were stained with uranyl and lead salts and imaged in an LEO 912 AB energy-filtered transmission electron microscope operated at 120 kV.

QUANTIFICATION AND STATISTICAL ANALYSIS

Analysis of FRA1 Motility

The motility of FRA1(707)-GFP particles along rhodamine-labeled microtubules in vitro was analyzed using the Multiple Kymograph plugin in Fiji (Schindelin et al., 2012). Immotile particles appear as vertical lines in the kymographs, whereas motile particles appear as diagonal lines. The motility index was calculated relative to the MBP alone control. Data were plotted using GraphPad Prism and statistical significance of data were calculated using the Student's t test.

Developmental Cell, Volume 44

Supplemental Information

Importin- β Directly Regulates the Motor Activity and

Turnover of a Kinesin-4

Anindya Ganguly, Logan DeMott, Chuanmei Zhu, Daniel D. McClosky, Charles T. Anderson, and Ram Dixit

SUPPLEMENTAL DATA

FIGURE S1

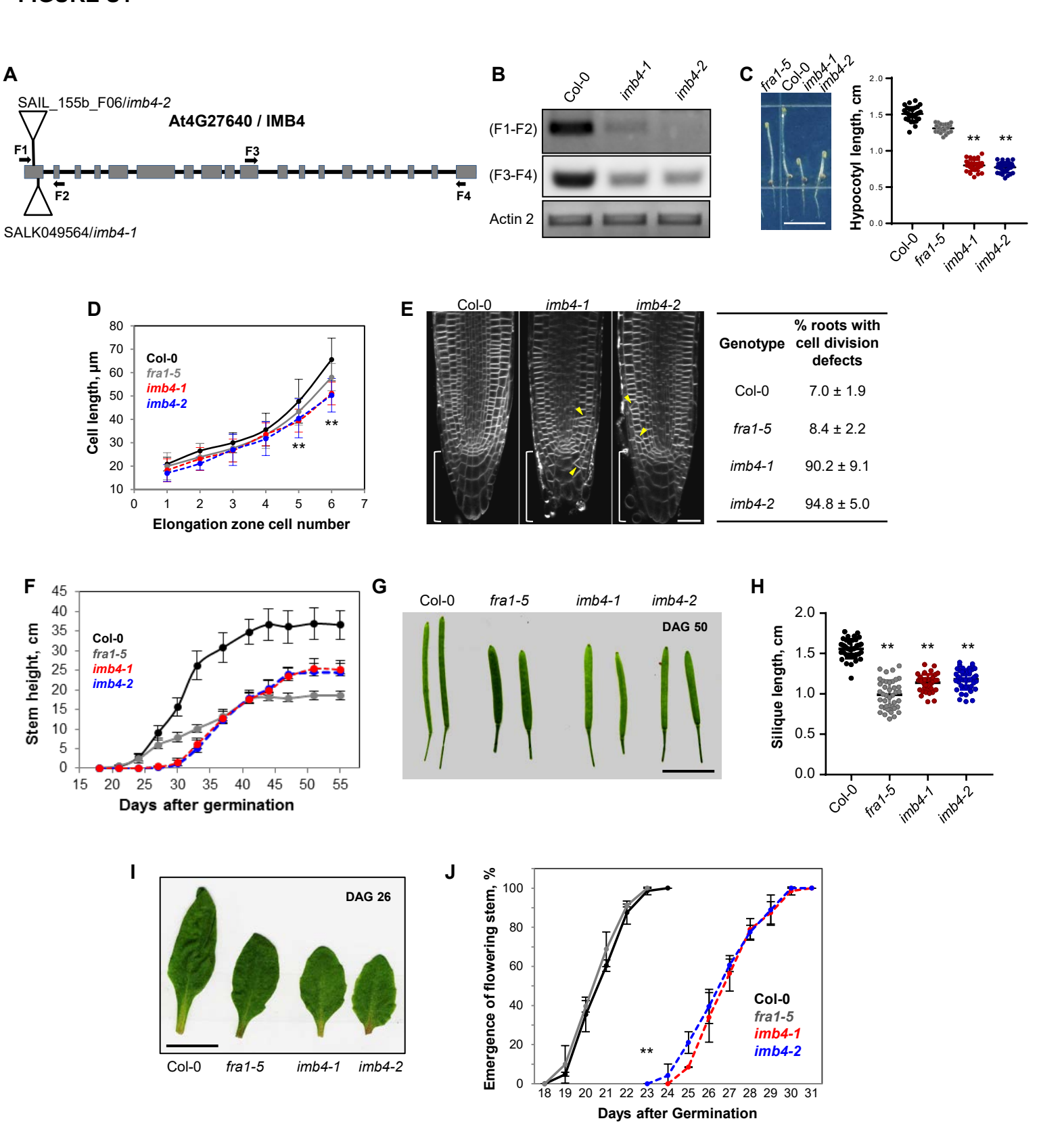


Figure S1. Phenotype of imb4 loss-of-function mutants, related to Figures 1 and 2

- (A) Schematic representation of the two independent T-DNA insertional mutants of the *IMB4* gene. Both of these mutants contain a T-DNA insertion within the first exon.
- (B) Semi-quantitative RT-PCR analysis of the *IMB4* transcript level in both *imb4* mutants compared to Col-0 control. The location of the F1-F4 primers in shown in (A).
- (C) Hypocotyl lengths of 4-day-old seedlings grown under dark conditions. Values are means \pm S.D. (n > 30 seedlings).
- (D) Epidermal cell lengths in the root elongation zone of 4-day-old seedlings. Cells were visualized by treating the roots with 5 μ M FM4-64 for 10 min. Cells in the root elongation zone are numbered from the rootward to shootward direction. Values are means \pm S.D. (n > 12 roots).
- (E) Cell division in the root meristem zone of 4-day-old seedlings visualized by treating the roots with 5 μ M FM4-64 for 10 min. Brackets indicate the region of the quiescent center and columella cells. The planes of cell division and cellular organization around the quiescent center were abnormal in the *imb4* mutants compared to wild type. Yellow arrowheads point to abnormal cell division planes. Scale bar = 20 μ m. The accompanying table shows the percentage \pm S.D. of roots with visible cell division defects (n = 20-22 roots per genotype).
- (F) Growth curves of the primary inflorescence stem. Values are means \pm S.D. (n = 28-31 plants). Unlike the *fra1-5* mutant, where inflorescence stems emerged at the same time as wild type but grew more slowly, the *imb4* mutants show delayed emergence of primary inflorescence stems but only slightly lower stem growth rates than wild type, albeit with stem growth halting at a shorter height than wild type.
- (G, H) Representative images and quantification of the length of mature siliques 50 days after germination (DAG). Values are means \pm S.D. (n = 35-40 siliques). Scale bar = 0.5 cm.
- (I) Size and shape of rosette leaves of one-month old plants. Scale bar = 0.5 cm.
- (J) Inflorescence stem emergence frequency in plants grown under continuous light. Values are means \pm S.D. (n = 30-32 plants).

Asterisks indicate significant differences between Col-0 and the imb4-1 and imb4-2 mutants as determined by Student's t test, ** p < 0.001.

FIGURE S2

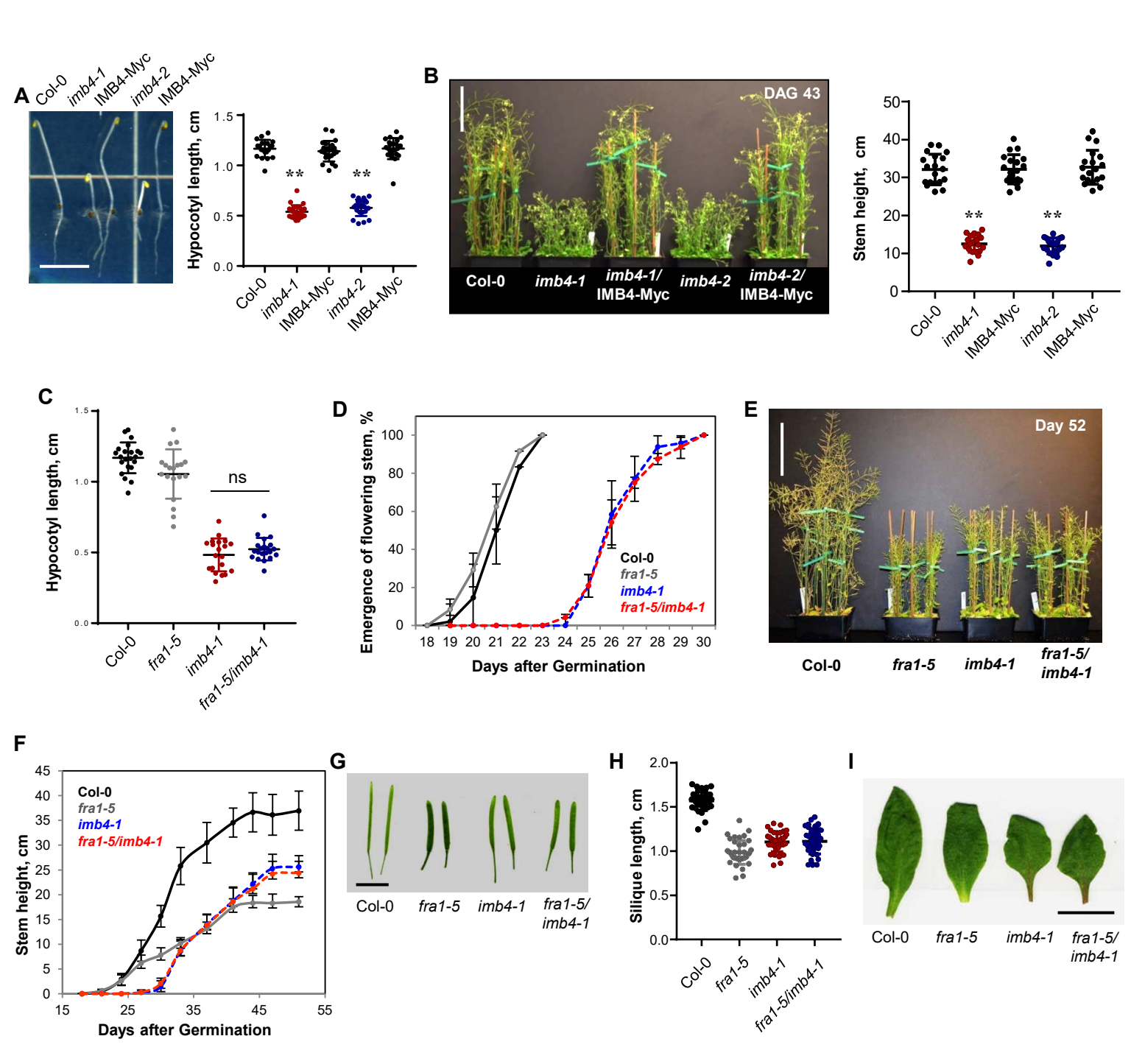


Figure S2. IMB4 is epistatic to FRA1, related to Figure 2

- (A) Hypocotyl lengths of 3-day-old seedlings grown under dark conditions. Both the *imb4* mutants were complemented with a *proIMB4::IMB4-Myc* construct. IMB4 cDNA was used to make the *IMB4-Myc* construct and genomic DNA was used for the *IMB4* promoter. Values are means \pm S.D. (n > 30 seedlings). Scale bar = 0.5 cm.
- (B) Whole-plant appearance and quantification of stem heights of plants 43 days after germination (DAG). Values are means \pm S.D. (n = 14-18 plants). Scale bar = 10 cm.
- (C) Hypocotyl lengths of 3-day-old dark-grown seedlings. Values are means \pm S.D. (n > 30 seedlings).
- (D) Inflorescence stem emergence frequency in plants grown under continuous light. Values are means \pm S.D. (n = 28-31 plants).
- (E, F) Whole-plant appearance and growth curves of plants grown under continuous light. Values are means \pm S.D. (n > 15 plants). Scale bar = 10 cm.
- (G, H) Representative images and quantification of the length of mature siliques 50 days after germination (DAG). Values are means \pm S.D. (n = 35-40 siliques). Scale bar = 0.5 cm.
- (I) Size and shape of rosette leaves of one-month old plants. Scale bar = 0.5 cm.
- Asterisks indicate significant differences as determined by Student's t test, ** p < 0.001.

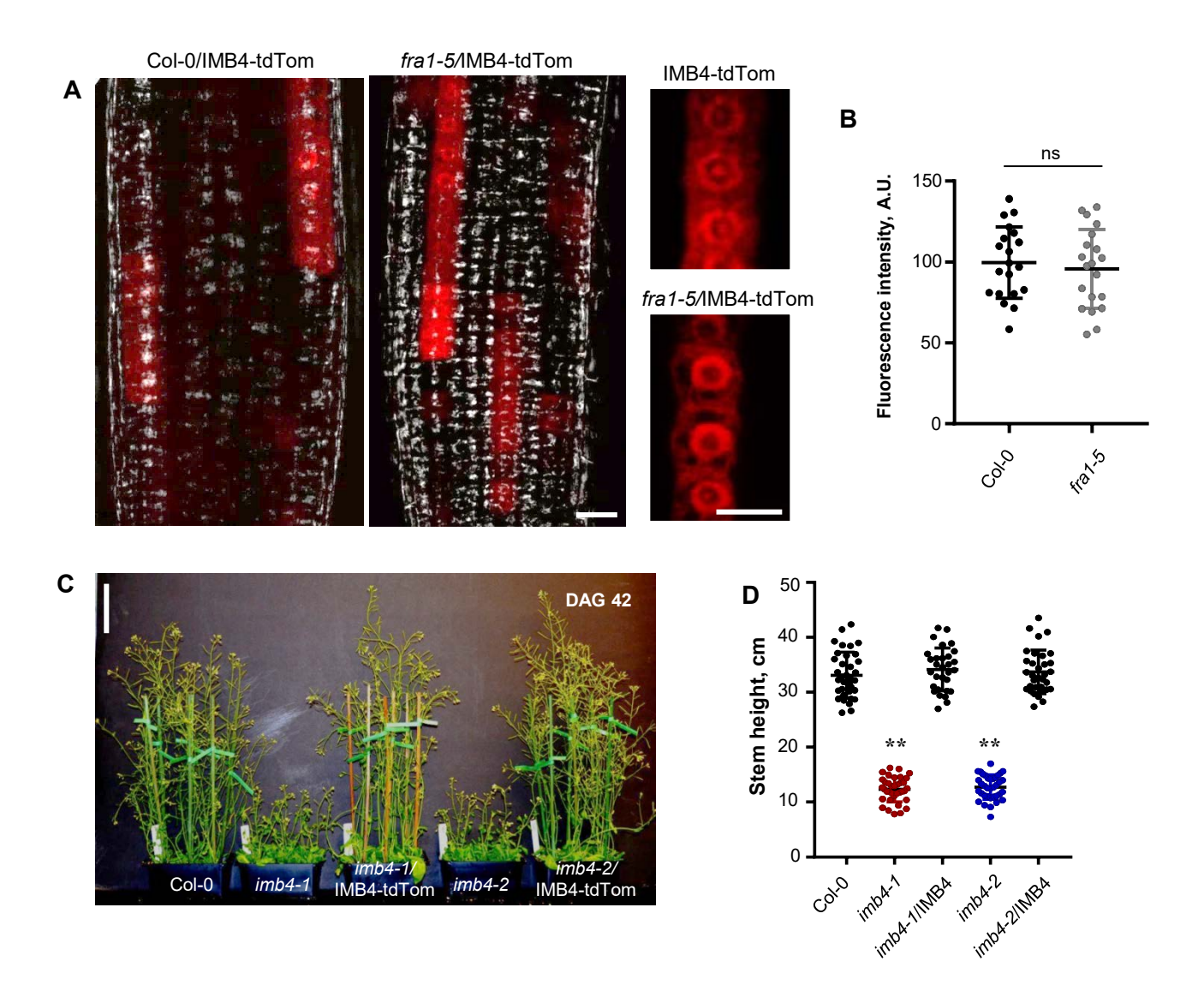


Figure S3. Complementation of the *imb4* loss-of-function mutants by IMB4-tdTomato, related to Figure 3

- (A) Representative images of IMB4-tdTomato in the roots of Col-0 and fra1-5 plants. Higher magnification views are shown to the right. Scale bar = $20 \mu m$.
- (B) Quantification of the IMB4-tdTomato fluorescence signal in cells from the roots of Col-0 and fral-5 plants. Values are means \pm S.D.
- (C, D) Whole-plant appearance and quantification of stem heights of *imb4* mutants complemented with the *proIMB4::IMB4-tdTomato* construct 42 days after germination (DAG). Values are means \pm S.D. (n = 34-36 plants). Scale bar = 10 cm. Asterisks indicate significant differences as determined by Student's *t* test, ** p < 0.001.

FIGURE S4

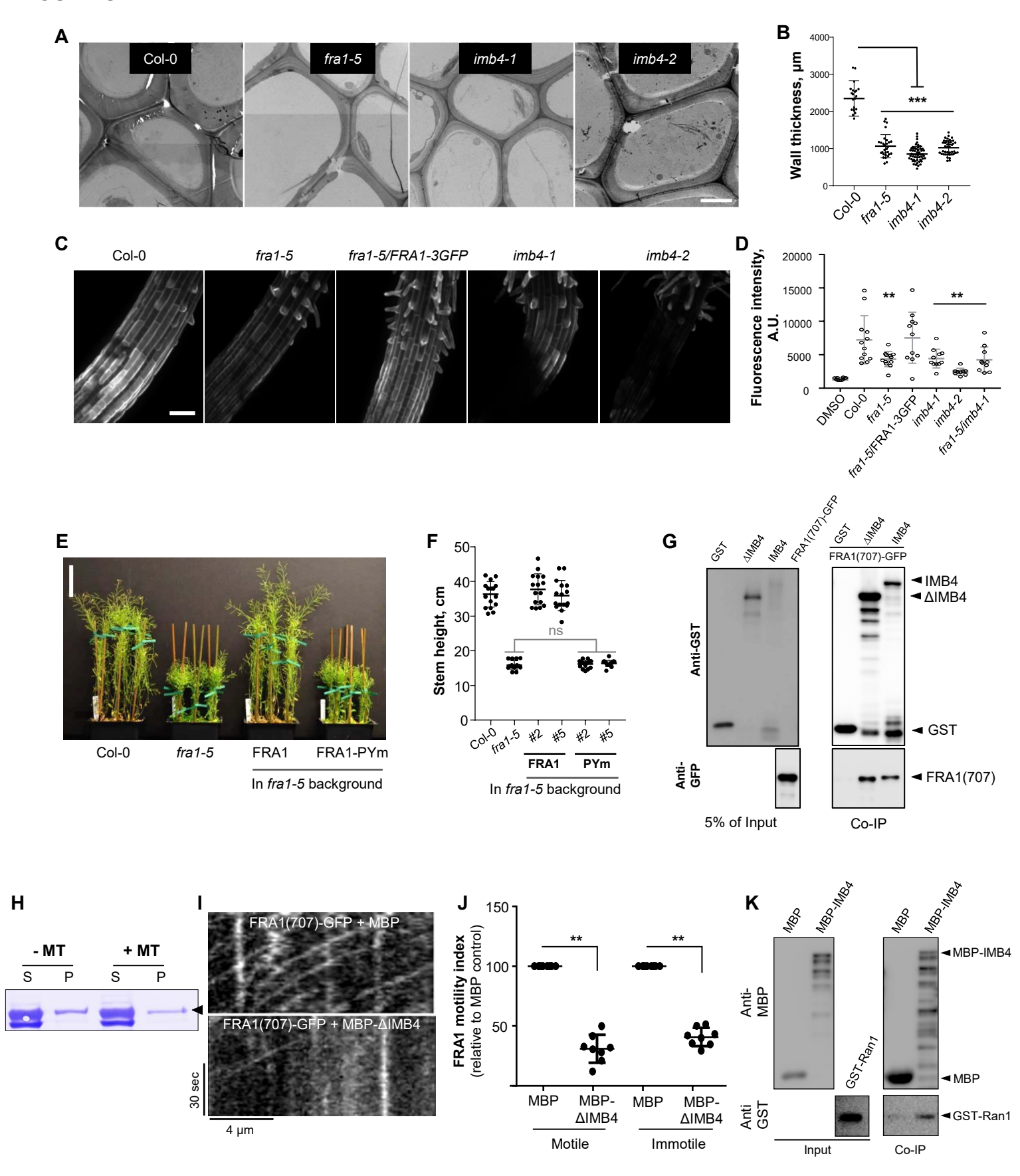


Figure S4. IMB4 binding to the FRA1 motor domain inhibits its activity, related to Figure 4

- (A and B) Transmission electron micrographs and quantification of the cell wall thickness of interfascicular fiber cells in basal stems. The electron micrographs are mosaics of images collected across stem cross sections. Values are means \pm S.D. (n = 20 cells for Col-0, 28 cells for *fra1-5*, 45 cells for *imb4-1* and 41 cells for *imb4-2*). Scale bar = 2 μ m.
- (C and D) Fluorescence images and quantification of fucose alkyne-labeled pectin reacted with Alexa 488-azide in the cell wall. The solvent dimethyl sulfoxide (DMSO) is used as a negative control. Pectin is synthesized in Golgi bodies and FRA1 is thought to transport Golgi-derived vesicles containing fucose alkyne-labeled pectin for secretion along cortical MTs (Zhu et al., 2015). Loss of FRA1 in the *fra1-5* mutant and reduction of FRA1 levels in the *imb4* mutants is associated with reduced pectin secretion into the cell wall. Values are means \pm S.E.M. (n > 6 cells per seedling 9-10 seedlings per treatment from two experiments). Scale bar = 10 μ m.
- (E, F) Whole-plant appearance and quantification of stem heights of Col-0, fral-5 and fral-5 mutants expressing either native promoter-driven FRA1 or FRA1-PYm proteins. Bars plot means \pm S.D. (n >15 plants). Scale bar = 10 cm.
- (G) The FRA1(707)-GFP protein interacts with full-length IMB4 and a more soluble ΔIMB4 (amino acids 151-894) *in vitro*. Glutathione-sepharose beads were used to pull down the GST-tagged IMB4 proteins incubated with equal amounts of FRA1(707)-GFP. Immunoblotting was performed with the indicated antibodies to detect the IMB4 and FRA1 proteins. GST alone was used as a negative control.
- (H) Microtubule co-sedimentation assay with MBP-ΔIMB4 protein (arrowhead). S, supernatant. P, pellet.
- (I) Kymographs showing the movement of FRA1(707)-GFP *in vitro* in the presence of MBP or MBP-ΔIMB4 on rhodamine-labelled microtubules.
- (J) Quantification of the number of motile and non-motile FRA1(707)-GFP puncta on rhodamine-labeled microtubules. Values are means \pm S.D (n = 8 independent microtubules from 2 independent set).
- (K) *In vitro* pull-down assay with full-length IMB4 tagged with MBP and GST-Ran1. MBP is used as a negative control. Asterisks indicate significant differences as determined by Student's t test, ** p < 0.001, *** p < 0.0001.

Table S1. Oligonucleotides used in this study, related to STAR Methods and the Key Resource Table

Vector/purpose	DNA Template	Orientation	Primer Sequence	
pENTR11		Forward	TATAGGTACCGAATGGCGCAATCTCTCGAACTTCTG	
	IMB4	Reverse	TATAGCGGCCGCTCAACTCGTGGATGCAAACGCAGCG	
	FRA1	Forward	TATAGGTACCGAATGGAATCTACGCCGCCACC	
	(1-530)	Reverse	GAATTCGCCGTCAAACAGCTTCATTTC	
pCAMBIA1300	IMB4	Forward	CATTGTCGACAAGCATGGACCTGCAATTGCTGG	
	Promoter	Reverse	TATACCTAGGAGTTTGTTTGTTGATTGATCTCTCTCC	
	IMB4	Forward	TATACCTAGGATGGCGCAATCTCTCGAACTTCTG	
		Reverse	TATAACGCGTACTCGTGGATGCAAACGCAGCG	
	tdTomato	Forward	TATAACGCGTATGGTGAGCAAGGGCGAGG	
		Reverse	TATAACTAGTTTACTTGTACAGCTCGTCCATGCC	
IMB4 Genotyping	SALK049564	Forward	GGATTACCGGACATTGGGC	
		Reverse	CTCACAACATTAGCACTCGC	
	SAIL155BF06	Forward	AGC CAAAGGTGAAAATATTGCC	
		Reverse	CCTGAAACCTTATGAAACACGG	
	SALK-LB Reverse TGGTTCACGTAGTGGGCCATCG		TGGTTCACGTAGTGGGCCATCG	
	SAIL-LB	Reverse	GAATTTCATAACCAATCTCGATACAC	
	F1	Forward	GGATTACCGGACATTGGGC	
IMB4	F2	Reverse	CTCACAACATTAGCACTCGC	
RT-PCR	F3	Forward	GCAGCTCATGCTATCTTCCAGACTC	
	F4	Reverse	ACTCGTGGATGCAAACGCAGCG	
pCAMBIA1300	IMB4-MYC	Forward	TATACCTAGGATGGCGCAATCTCTCGAACTTCTG	
		Reverse	TATAACGCGT TTACAGATCTTCTTCAGAAATAAGTTT	
IMB4 promoter			TTGTTCACTCGTGGATGCAAACGCAGCG	
pCAMBIA2300	ECED	Forward	TATAACGCGTATGGTGAGCAAGGGCGAGG	
35S promoter	EGFP	Reverse	TATAGAGCTCTTACTTGTACAGC CGTCC	
pGEX-6P-1	IMB4	Forward	TATAGGATCCATGGCGCAATCTCTCGAACTTCTG	
		Reverse	TATAGCGGCCGCTCAACTCGTGGATGCAAACGCAGCG	
pGEX-6P-1	Ran1	Forward	TATGGATCCATGGCTCTACCTAACCAG	
		Reverse	TATGCGGCCGCTTACTCAAAGATATCATCATCG	
pGEX-6P-1	ΔIMB4	Forward	TATAGGATCCAACACATTTAGGCCATACTTTGCAG	
	(151-894)	Reverse	TATAGCGGCCGCTCATTTGCATAGCTCTCCAACAC	
pMAL-C5X	IMB4	Forward	TATACATATGATGGCGCAATCTCTCGAACTTCTG	
		Reverse	TATAGCGGCCGCTCAACTCGTGGATGCAAACGCAGCG	
pMAL-C5X	ΔIMB4	Forward	TATACATATGAACACATTTAGGCCATACTTTGCAG	
	(151-894)	Reverse	TATAGCGGCCGCTCATTTGCATAGCTCTCCAACAC	
pTEV	FRA1-PY-AA	Reverse	CTGTCTCTGGCGCAACATGGGCAC	
	FRA1-KR-AA	Reverse	CATGGGCACCATCTTTAGCCGCTTTCTCATCACCGA G	
	NACK1	Forward	TATACCATGGCCATGACTATAAAAACACCGGGAACTCC	
	(1-540)	Reverse	TATAGTCGACTTATTGAAGGTGTTCGAGTTTGCGG	
	POK1	Forward	TATACATATGATGTCCCGAAACGTTCCGAGAATAGAG	
pMAL-C5X	(1-500)	Reverse	TATAGTCGACTTATTGCGCGAACTTCAGGGTGCTG	
	KINUA	Forward	TATACCATGGCCATGTCAACGACTTCAGGAACCG	
•	(1-512)	Reverse	TATAGTCGACTTATCCAAGGGCAAGTCTTTCAGC	